國立臺灣大學工學院化學工程學研究所碩士論文

Graduate Institute of Chemical Engineering

College of Engineering

National Taiwan University

Master's Thesis

利用表面增強拉曼晶片建立一個檢測細胞膜上生物分子的平台

Using Surface-Enhanced Raman Spectroscopy Chips to Detect Biomolecules on Cell Membrane Platforms

吳伯安

Po-An Wu

指導教授：趙玲 博士

Advisor: Ling Chao, Ph.D.

中華民國 113 年 7 月

July , 2024

doi:10.6342/NTU202403291

口試委員會審定書

國立臺灣大學碩士學位論文

口試委員會審定書

MASTER'S THESIS ACCEPTANCE CERTIFICATE
NATIONAL TAIWAN UNIVERSITY

利用表面增強拉曼晶片建立一個檢測細胞膜上生物分子的平台

Using Surface-Enhanced Raman Spectroscopy Chips to Detect Biomolecules on Cell Membrane Platforms

本論文係 吳伯安 (姓名) R11524119 (學號) 在國立臺灣大學 化學工程 (系/所/學位學程)完成之碩士學位論文，於民國 113 年 7 月 22 日承下列考試委員審查通過及口試及格，特此證明。

The undersigned, appointed by the Department / Graduate Institute of Chemical Engineering on 22 (date) 7 (month) 113 (year) have examined a Master's Thesis entitled above presented by Po-An Wu (name) R11524119 (student ID) candidate and hereby certify that it is worthy of acceptance.

口試委員 Oral examination committee:

趙玫　謝之真　廖英志

（指導教授 Advisor）

系（所、學位學程）主管 Director: 廖英志

doi:10.6342/NTU202403291

誌謝

首先，最感謝的人絕對是教導我研究的趙玲老師，在我常常沒有明確方向時，總是能夠提點我，使我了解到自己在研究上的嚴謹程度還有很大的進步空間。

再來，感謝哲綸、子慈、孟楷三位學長姐，在我不了解研究想法的正確性時，總是能夠給予我良好的建議，讓我更加懂得研究過程中的邏輯。

接著，感謝奕寬和奕惟兩位好夥伴，在實驗上有器材問題時都能及時幫助我避免實驗開天窗。在研究不順利時，也願意和我討論困難點，才能讓我順利度過難關。

還要感謝學弟妹們，謝謝雅榆在我口試前焦頭爛額的時候，幫我處理好環安衛的事情。謝謝桓彰在我實驗進度緊湊時，幫我配置緩衝溶液。謝謝柏諺幫我處理部分的口試數據，讓我節省了不少時間。謝謝優美、翊涵在我口試前，總是幫我加油。

另外，謝謝幫我 SEM 委測的許小姐，雖然我的樣品很麻煩，但您還是不厭其煩的幫我處理，甚至晚上還加班，就為了給我可以解釋的數據。您也常常鼓勵我要勇敢面對困難，使我有動力堅持下去。

最後，感謝在這兩年內在學業或研究上有幫助過我的人，希望大家都能夠研究順利。最重要的是，希望大家在努力生活之餘都能夠開開心心的度過每一天!!

doi:10.6342/NTU202403291

摘要

細胞膜上的物質傳輸、識別和結合與各種生理機制密切相關。我們建立了一種基於支撐細胞膜的拉曼技術檢測平台來研究細胞膜上的事件。通過將細胞膜鋪設在具有拉曼增強結構的基材上，利用拉曼光譜檢測細胞膜及其相互作用的物質。由於細胞膜只有奈米級的厚度，上面只有少量的蛋白質和與其作用的物質，我們使用膠體粒子阻擋後鍍金形成的金三角結構晶片來增強訊號，並研究不同電漿製程參數對晶片結構的影響，以進一步改善晶片增強訊號的能力，也找到了適當的雷射參數以避免生物分子在實驗過程中被破壞。我們首先在增強晶片上分別檢測霍亂毒素次單元 B (CTB)、1,2-二油酰-sn-甘油-3-磷酸膽鹼(DOPC)脂雙層膜和巨大質膜囊泡膜片(GPMV patch)的訊號。實驗結果顯示，我們成功在增強晶片上獲得了霍亂毒素次單元 B 和 1,2-二油酰-sn-甘油-3-磷酸膽鹼脂雙層膜的訊號，這些訊號與標準品的拉曼訊號具有一致性。然而，巨大脂質膜囊泡膜片(GPMV patch)的訊號卻非常微弱，其特徵峰位置與標準品不一致。這可能是因為此研究的增強晶片是由膠體粒子阻擋後鍍金形成的金三角結構晶片，訊號增強顯著發生在約 100 奈米寬的尖角隙縫區域。霍亂毒素次單元 B 的分子大小約為 100 奈米，能夠進入這些空隙，從而增強訊號。之前文獻也指出，1,2-二油酰-sn-甘油-3-磷酸膽鹼脂雙層膜能鋪於增強晶片底部，並進入增強區域，以造成訊號增強。然而，當 20 微米大小的巨大脂質膜囊泡鋪於增強基材形成膜片時，細胞膜的張力很可能會使膜片懸浮在金三角結構上，而難以落入尖角增強區域，從而導致訊號微弱。我們進一步分別使用 1,2-二油酰-sn-甘油-3-磷酸膽鹼脂雙層膜內加入的單唾液酸四己糖神經節苷脂(GM1)，以及巨大質膜囊泡膜片內的天然受體來捕捉霍亂毒素次單元 B 至膜片上，以了解這些膜片配合目前拉曼增強基材能否做為檢測器的可能性。經由實驗組和控制組相扣處理後的訊號顯示，在 1,2-二油酰-sn-甘油-3-

doi:10.6342/NTU202403291

磷酸膽鹼脂雙層膜上捕捉到的霍亂毒素次單元 B 可被檢測到，但由巨大質膜囊泡膜片捕捉到的霍亂毒素次單元 B 的訊號則是微弱難以辨別。這結果也符合我們對於 1,2-二油酰-sn-甘油-3-磷酸膽鹼脂雙層膜和巨大質膜囊泡膜片所坐落的位置的推測，當霍亂毒素次單元 B 黏到 1,2-二油酰-sn-甘油-3-磷酸膽鹼脂雙層膜上時，霍亂毒素次單元 B 仍能位於金三角尖角空隙之間，但當霍亂毒素次單元 B 黏到巨大脂質膜囊泡膜片上時，霍亂毒素次單元 B 則會遠離訊號增強區域，導致其無法被偵測到。

關鍵字：支撐式細胞膜，表面增強拉曼光譜，霍亂毒素次單元 B，1,2-二油酰-sn-甘油-3-磷酸膽鹼，奈米金三角

doi:10.6342/NTU202403291

Abstract

The transport, recognition, and binding of substances on cell membranes are closely related to various physiological mechanisms. We established a detection platform based on Raman technology with supported cell membranes to study events on cell membranes. By depositing cell membranes on substrates with Raman-enhanced structures, we used Raman spectroscopy to detect cell membranes and their interacting substances. Since cell membranes are only nanometer-thick, with only a small number of proteins and interacting substances on them, we used gold nanotriangle structure chips formed by colloidal lithography to enhance the signal. We studied the impact of different plasma processing parameters on the chip structure to further improve the chip's signal enhancement capability, and also found appropriate laser parameters to avoid damaging biomolecules during the experiment. We first detected the signals of cholera toxin subunit B (CTB), 1,2-dioleoyl-sn-glycero-3-phosphocholine (DOPC) lipid bilayer, and giant plasma membrane vesicle (GPMV) patches on the enhancement chip. The experimental results showed that we successfully obtained the signals of CTB and DOPC lipid bilayer on the enhancement chip, which were consistent with the Raman signals of the standards. However, the signal of the GPMV patch was very weak, and its

doi:10.6342/NTU202403291

characteristic peak position was inconsistent with the standard. This could be because the enhancement chip used in this study was a gold nanotriangle structure chip, with significant signal enhancement occurring in the narrow gaps of about 100 nanometers. The size of the CTB molecule is about few nanometers, allowing it to enter these gaps and thus enhance the signal. Previous literature has also pointed out that the DOPC lipid bilayer can form at the bottom of the enhancement chip and enter the enhancement area to cause signal enhancement. However, when the 20-micron-sized GPMV forms a patch on the enhancement substrate, the membrane tension is likely to suspend the patch on the gold triangular structure, making it difficult to fall into the narrow enhancement area, resulting in a weak signal. We further used DOPC lipid bilayers with monosialotetrahexosylganglioside (GM1) and GPMV patches with natural receptors to capture CTB onto the patches to explore the potential of these patches as sensors. The signal processed by experimental and control groups showed that CTB captured on DOPC lipid bilayer could be detected, but the signal of CTB captured by the GPMV patch was weak and difficult to distinguish. This result also aligns with our hypothesis about the positions of the DOPC lipid bilayer and GPMV patch. When CTB adheres to the 1,2-dioleoyl-sn-glycero-3-phosphocholine lipid bilayer, it remains in the gap between the gold triangular tips, but when it adheres to the GPMV patch, CTB could be

doi:10.6342/NTU202403291

far from the signal enhancement area, making it undetectable in our current chip.

Keywords：Cell membrane patch, Raman spectroscopy, Cholera toxin subunit B, 1,2-Dioleoyl-sn-glycero-3-phosphocholine, Gold nanotriangle

doi:10.6342/NTU202403291

Table of Content

doi:10.6342/NTU202403291

doi:10.6342/NTU202403291

doi:10.6342/NTU202403291

Figure Captions

doi:10.6342/NTU202403291

doi:10.6342/NTU202403291

doi:10.6342/NTU202403291

doi:10.6342/NTU202403291

Figure 3-16 The impact of the detection platform fabrication process on the spectral acquisition of DOPC-supported lipid bilayers. (a) and (b) upside down measurements on chips treated with Ar-plasma for 10 minutes, using polystyrene microparticles from Bang Laboratories and GmbH, respectively. (c) and (d) upside down measurements on chips treated with Ar-plasma for 10 minutes followed by additional air-plasma treatment for 20 seconds, using polystyrene microparticles from Bang Laboratories and GmbH, respectively. (e) and (f) upside up measurements on chips treated with Ar-plasma for 10 minutes followed by additional air-plasma treatment for 20 seconds, using polystyrene microparticles from Bang Laboratories and GmbH, respectively. Process to obtain spectrum of DOPC with 1 mol% GM1 on chips. process to obtain spectrum of DOPC on chips. (1) and (2) the spectra of (DOPC (with GM1) + PBS buffer + chip) and (PBS buffer + chip) before background removal. (3) and (4) the spectra of (DOPC (with GM1) + PBS buffer + chip) and (PBS buffer + chip) after background removal using a 5th-degree polynomial. (5) and (6) the spectra of (DOPC (with GM1) + PBS buffer + chip) and (PBS buffer + chip) after background removal using a 5th-degree

doi:10.6342/NTU202403291

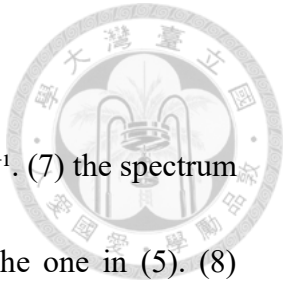

doi:10.6342/NTU202403291

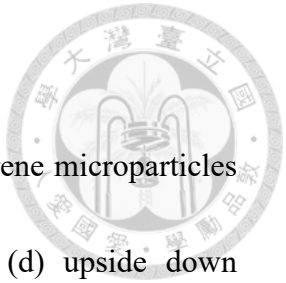

doi:10.6342/NTU202403291

doi:10.6342/NTU202403291

doi:10.6342/NTU202403291

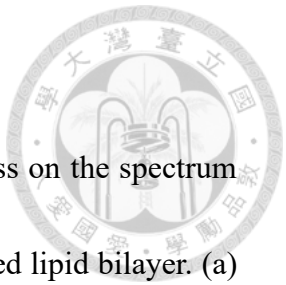

Figure 3-25 The impact of the detection platform fabrication process on the spectrum acquisition of CTB on an enhanced chip with a DOPC-supported lipid bilayer. (a) and (b) upside down measurements on chips treated with Ar-plasma for 10 minutes, using polystyrene microparticles from Bang Laboratories and GmbH, respectively. (c) and (d) upside down measurements on chips treated with Ar-plasma for 10 minutes followed by additional air-plasma treatment for 20 seconds, using polystyrene microparticles from GmbH and Bang Laboratories, respectively. (e) and (f) upside up measurements on chips treated with Ar-plasma for 10 minutes followed by additional air-plasma treatment for 20 seconds, using polystyrene microparticles from Bang Laboratories and GmbH, respectively. process to obtain spectrum of CTB with DOPC containing 1 mol% GM1 on chips. (1)(2) the spectra of (CTB + DOPC(with GM1) + PBS buffer + chip) and (DOPC(with GM1) + PBS buffer + chip) before background removal. (3)(4) the spectra of(CTB + DOPC(with GM1) + PBS buffer + chip) and (DOPC(with GM1) + PBS buffer + chip) after background removal using a 5th-degree polynomial. (5)(6) the spectra of (CTB + DOPC(with GM1) + PBS buffer + chip) and (DOPC(with GM1) + PBS buffer + chip) after background removal using a 5th-degree polynomial, followed by normalization at wavenumber 720 cm^{-1}. (7) the spectrum of CTB obtained by

doi:10.6342/NTU202403291

doi:10.6342/NTU202403291

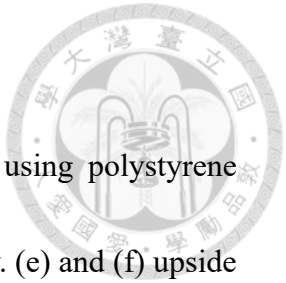

doi:10.6342/NTU202403291

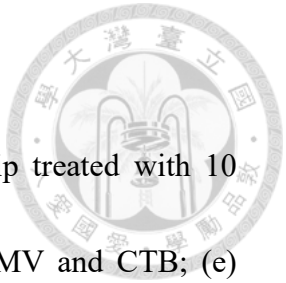

Table Captions

doi:10.6342/NTU202403291

Chapter 1 Introduction

1.1 Overview

The cell membrane, serving as the boundary between cells and their external environment, plays a crucial role in protecting cells from harm and remains a pivotal area for scientists to understand some disease characteristics. Therefore, comprehending how the cell membrane proteins, recognizes, and binds substances is crucial. Scientists have developed various kinds of sensors to study the membrane proteins and the ligand binding with these membrane proteins. In this study, we deposited cell membranes on a Raman-enhanced substrate and utilized Raman spectroscopy as a transducer to detect the membrane components and the ligand binding to the cell membrane.

1.2 Supported Lipid Bilayers

Our cell membranes are derived from Giant Plasma Membrane Vesicles (GPMVs), induced from Hela cells through a chemical vesiculation process using paraformaldehyde (PFA) and dithiothreitol (DTT). Subsequently, depositing these vesicles onto the substrate surface allows for the formation of membrane patches in their natural environment. The main component of the cell membrane is the phospholipid bilayer, which also contains

doi:10.6342/NTU202403291

various types of membrane proteins, including integral proteins and peripheral proteins. Additionally, there are glycans and glycolipids responsible for recognizing foreign substances. Cholesterol is also present in animal cell membranes to stabilize the membrane structure[1].

1.3 Raman Spectroscopy

1.3.1 Raman Spectroscopy

When laser illumination is applied to different biomolecules, it produces Raman scattering at various wavelengths, allowing for the acquisition of chemical bonding information and biological fingerprint characteristics. Furthermore, the Raman signal of water is weak in the wavenumber range of 600 to 1800 cm-1, making Raman spectroscopy highly suitable as a transducer for detecting biomolecules in their native environment. Raman scattering can be categorized into three types, as shown in **Figure 1-1** : Rayleigh scattering, Stokes Raman scattering, and anti-Stokes Raman scattering. Due to the extremely weak nature of anti-Stokes Raman scattering, Raman spectroscopy primarily detects the frequency differences between Rayleigh scattering and Stokes Raman scattering. The frequency shift between Stokes Raman scattering and the incident light is related to molecular vibrations, and different substances exhibit unique molecular

doi:10.6342/NTU202403291

vibration modes. This characteristic makes Raman spectroscopy suitable for analyzing various substances.

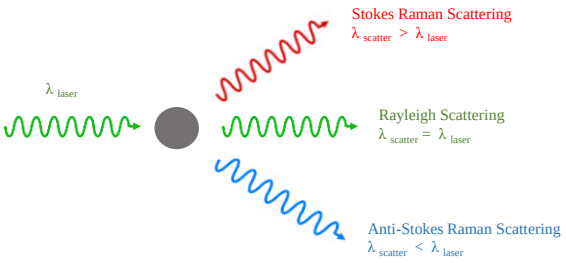

Figure 1-1 Raman scattering schematic.

1.3.2 Surface-Enhanced Raman Spectroscopy (SERS)

Due to the extremely low probability of spontaneous Raman scattering, where only about one in a hundred million photons participate, various techniques have been developed to enhance the likelihood of Raman scattering. One such technique we use is Surface-Enhanced Raman Spectroscopy (SERS), which is based on localized surface plasmon resonance (LSPR).

The principle behind LSPR involves a beam of light striking a metal surface and exciting surface plasmons. These plasmons then oscillate collectively and coherently. When the frequency of these oscillations aligns with the frequency of the incident light, resonance occurs, leading to the strongest interaction, known as surface plasmon resonance. Additionally, at the nanoscale, these surface plasmons are confined to the area around the tiny metal structures and cannot travel along the interface. This specific type

doi:10.6342/NTU202403291

of surface plasmon resonance is called localized surface plasmon resonance (LSPR). By enhancing the local electric field in this manner, the Raman signal can be significantly amplified. Common materials used include gold, platinum, silver, and copper. Nanostructures made from these metals induce plasmon resonance effects that increase the likelihood of Raman scattering. In our case, we coat a glass slide with a layer of gold nanotriangles. The vertices of these nanotriangles are known as "hot spots." When the vertices of adjacent gold nanotriangles are close enough, they induce an enhanced local electric field, which in turn amplifies the Raman signal.

1.4 Cholera Toxin Subunit B (CTB)

The B subunit of cholera toxin is the non-toxic portion of the toxin and consists of a pentameric structure composed of five monomers[2](refer to **Figure 1-2**). To confirm the feasibility of surface-enhanced Raman spectroscopy (SERS) chips and GPMV patches, we selected cholera toxin subunit B (CTB) as the analyte. The reason is that the specific binding between CTB and the ganglioside receptor GM1 is well-established[2], and GM1 is present in HeLa cells.

doi:10.6342/NTU202403291

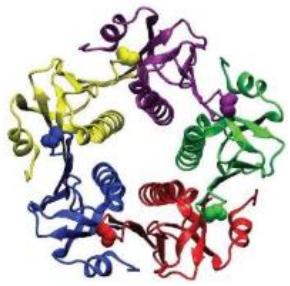

Figure 1-2 Illustration of the structure of cholera toxin subunit B.

Chapter 2 Materials and Methods

2.1 Materials

(1) Polydimethylsiloxane (PDMS; Sylgard 184) from Corning (Corning, NY, USA)

(2) Falcon™ cell culture dishes from Fisher Scientific (Waltham, MA USA). Taiwan distributor: 騰達行企業股份有限公司，(02) 2720-2215

(3) Glass coverslip from VWR (Radnor, PA, USA).

(4) Polystyrene(Mean Diameter:0.31μm ,10.1%Solids).Polystyrene from Bangs Laboratories Inc (Fishers, IN, USA). Taiwan distributor: 美商欣科寶利股份有限公司 (02) 8712-0600

(5) Polystyrene(Mean Diameter:0.31μm ,10%Solids).Polystyrene from microParticles GmbH (Berlin, IN, Germany)

(6) Ethanol from Sigma-Aldrich (St. Louis, MO, USA). Taiwan distributor: 友和貿易股份有限公司，(02) 2600-0611

doi:10.6342/NTU202403291

(7) Sodium chloride from Sigma-Aldrich (St. Louis, MO, USA). Taiwan distributor: 友和貿易股份有限公司，(02) 2600-0611

(8) Potassium chloride from Sigma-Aldrich (St. Louis, MO, USA). Taiwan distributor: 友和貿易股份有限公司，(02) 2600-0611

(9) Sodium phosphate dibasic from Sigma-Aldrich (St. Louis, MO, USA). Taiwan distributor: 友和貿易股份有限公司，(02) 2600-0611

(10) Sodium phosphate monobasic from Sigma-Aldrich (St. Louis, MO, USA). Taiwan distributor: 友和貿易股份有限公司，(02) 2600-0611

(11) 3,3'-Dilinoleyloxacarbocyanine perchlorate (Fast-DiO) from Invitrogen (Waltham, MA, USA). Taiwan distributor: Life Technologies CO., Ltd., (02) 2358-2838

(12) HEPES (4-(2-hydroxyethyl)-1-piperazineethanesulfonic acid) from Sigma-Aldrich (St. Louis, MO, USA). Taiwan distributor: 友和貿易股份有限公司，(02) 2600-0611

(13) Calcium chloride from Sigma-Aldrich (St. Louis, MO, USA). Taiwan distributor: 友和貿易股份有限公司，(02) 2600-0611

(14) Dithiothreitol (DTT) from Sigma-Aldrich (St. Louis, MO, USA). Taiwan distributor: 友和貿易股份有限公司，(02) 2600-0611

(15) Paraformaldehyde (PFA) from Sigma-Aldrich (St. Louis, MO, USA). Taiwan distributor: 友和貿易股份有限公司，(02) 2600-0611

doi:10.6342/NTU202403291

(16) Cholera toxin subunit B from Invitrogen (Waltham, MA, USA). Taiwan distributor: Life Technologies CO., Ltd., (02) 2358-2838

2.2 Apparatus

(1) PDC-32G plasma cleaner, Harrick Plasma (Ithaca, NY, USA). Taiwan distributor: 翰揚貿易股份有限公司，(02) 2232-7158

(2) Direct-Q® 3 UV water purification, 台灣默克股份有限公司 Merck Millipore (Taiwan)，(02)2162-1111

(3) Hettich Mikro 120 microliter centrifuge from Hettich Lab Technology (Föhrenstr. 12, Tuttlingen, Germany).

(4) Ultrasonic cleaner from 雷伯斯儀器有限公司(Yangmei, Taoyuan, Taiwan)，(03) 488-3326

(5) Ultrasonic cleaner from 見誠科技有限公司(Zhongshan, Taipei, Taiwan)，(02)7701-5804

(6) Spin coating machine from Top Tech (Dali, Taichung, Taiwan). (04) 2406-1658

(7) Electron-beam evaporator from Complex for Research Excellence (Zhongzheng, Taipei, Taiwan). (02) 3366-3366

(8) FEI Ultra-High Resolution FE-SEM with low vacuum mode from UNIVERSITY

doi:10.6342/NTU202403291

OF NORTH TEXAS (Denton, Texas, USA)

(9) IX81 motorized inverted microscope, Olympus (Tokyo, Japan). Taiwan distributor: 元利儀器股份有限公司，(02) 8751-2222

(10) IX83 motorized inverted microscope, Olympus (Tokyo, Japan). Taiwan distributor: 元利儀器股份有限公司，(02) 8751-2222

(11) Hamamatsu ORCA-R2 digital CCD camera, Hamamatsu (Iwata, Japan). Taiwan distributor: 台灣濱松光子學有限公司，(07) 2620735

(12) Direct heat type CO2 and tris-gas incubator from Astec Co., Ltd. (Kasuya, Japan). Taiwan distributor: 弘優科技有限公司，(02) 8531-5386

(13) Water bath from 裕德科技有限公司 (Zhonghe, New Taipei City, Taiwan)，(02) 2226-7636

(14) inVia Raman microscope, Renishaw (Gloucestershire, UK). Taiwan distributor: 友德國際股份有限公司 ，(02)2799-3399

(15) He-Ne 633nm laser, Renishaw (Gloucestershire, UK). Taiwan distributor: 友德國際股份有限公司 ，(02)2799-3399

2.3 Fabrication of Gold Nanotriangle Substrates Based on Nanosphere Lithography

doi:10.6342/NTU202403291

2.3.1 Deposition of Polystyrene Microparticles on Substrates by Spin Coating

To achieve a uniform monolayer arrangement of polystyrene microparticles in a Hexagonal Close Packing (HCP) formation on a glass slide, we needed to ensure the glass surface is clean and the polystyrene microparticles are uniformly distributed in the solution. First, we rinsed 24x30 mm glass slides with 95% ethanol and DI water, and then cleaned them using Argon plasma (power set to HIGH) for 10 minutes to ensure the surface is nearly free of impurities. Next, we centrifuged 700 μL of the original polystyrene microparticle solution (300 nm in diameter) at 9500 rpm for 15 minutes. 580μl and 475μl of supernatants were removed from the centrifuged microparticle solutions from GmbH and Bang Laboratory, respectively. Then, 900 μL and 1600 μL of mixture of water and ethanol (volume ratio =1:1) were added to resuspend the particles from GmbH and Bang Laboratory, respectively.

Once all materials were prepared, we set the spin coater to 3000 rpm for 3 minutes, vortexed the resuspensions for 1 minute, and then sonicated them for 15 minutes to ensure the uniformity of the polystyrene microparticles in the resuspensions. Next, we fixed the cleaned glass slide on PDMS, and added the resuspensions, allowing them to sit for 4 minutes (reducing the time by 5 seconds for each subsequent slide). Then, we performed

doi:10.6342/NTU202403291

spin coating to obtain a monolayer of polystyrene microparticles arranged in a Hexagonal Close Packing (HCP) formation on the glass slide.

2.3.2 Cleaning the Substrate before Metal Deposition

To ensure that the surface of the gaps between the polystyrene microparticles are clean before metal deposition, the substrate underwent Ar-plasma cleaning for 20 minutes. The cleaning time was recorded to ensure that the interval between cleaning and metal deposition is around 2 hours. Finally, the slide with the coated polystyrene microparticles was fixed in the center of the wafer.

2.3.3 Metal Deposition

We use an electron beam evaporator for metal deposition. First, the wafer was fixed on the rotating stage, ensuring that each substrate was oriented consistently relative to the electron beam. Then, rotate the stage at an angle of 17 degrees and a speed of 5 rpm to ensure the uniformity of the metal layer. After the vacuum process, the metal deposition began at a rate of 0.1 Å/s, first depositing a 2.5 nm layer of Ti as an adhesion layer, followed by a 30 nm layer of Au.

doi:10.6342/NTU202403291

2.3.4 Polystyrene Microparticle Lift-off

After the metal deposition process, the polystyrene microparticles must be removed. First, the chip was placed in a clear glass bottle filled with 99.8% ethanol (**Figure 2-1**). Then, the three-liter sonicator shown in **Figure 2-2** was powered at 84W for 10 minutes to lift off the polystyrene microparticles. The process is complete when the chip changed from opaque to transparent. Finally, the wafer was cleaned with 95% ethanol and DI water, then dried with nitrogen gas. The wafer was stored in a Petri dish at room temperature and atmospheric pressure.

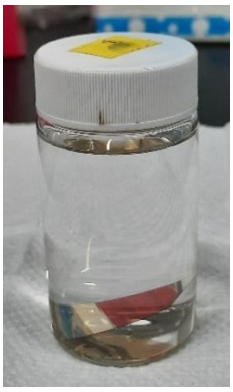

Figure 2-1 The chip is placed in bottles with solvents to lift-off the polystyrene microparticles.

(a) **(b)**

Figure 2-2 (a) The side view of the sonicator (b) Top view of the sonicator and

doi:10.6342/NTU202403291

arrangement of glass bottles in the sonicator.

2.4 Preparation of Polydimethylsiloxane (PDMS) wells

PDMS wells were made by mixing PDMS oligomers (Sylgard 184A) and PDMS crosslinkers (Sylgard 184B) at a 10:1 weight ratio. The mixture was then placed under vacuum until all bubbles were removed. Next, 1.2 ml of the mixed solution was pipetted into a mold made from a silicon wafer to create a PDMS film measuring 5 cm in length, 4 cm in width, and 0.55 mm in height. Finally, the mixture was cured in an oven at 75°C for 12 hours. After curing, the PDMS was used to create PDMS wells with a diameter of 1.3 cm using a hole puncher. The wells were then soaked in electronic-grade acetone and sonicated for 15 minutes. The wells were then placed in fresh acetone and left to sit for 12 hours, followed by another 15 minutes of sonication in fresh acetone. Finally, the wells were placed in an oven at 75°C for 12 hours to ensure the complete evaporation of the acetone before use.

2.5 Sample Preparation

2.5.1 Formation of Native Cell Membrane Platform

doi:10.6342/NTU202403291

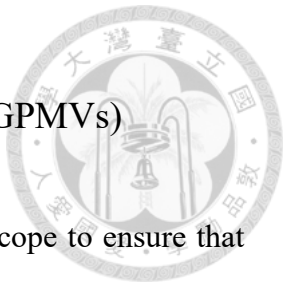

2.5.1.1 Preparation of Giant Plasma Membrane Vesicles(GPMVs)

Before the cells were used, they were observed under a microscope to ensure that their coverage in the culture dish was around 50% to 60%. The cell medium was removed and 2 ml of phosphate-buffered saline (PBS) (137 mM NaCl, 10 mM Na_2HPO_4, 2 mM NaH_2PO_4, and 2.7 mM KCl, pH 7.4) was added to the culture dish. The dish was swirled in a figure-eight motion 10 times, then the PBS was replaced with fresh buffer, and the HeLa cells were washed a total of three times. Next, the cells were stained with PBS containing 3,3'-Dilinoleyloxacarbocyanine perchlorate (Fast-DiO) at 4°C for 10 minutes. The cells were washed three times with 2 ml of PBS, followed by three washes with 2 ml of GPMV buffer (150 mM NaCl, 10 mM HEPES, 2 mM $CaCl_2$, pH 7.4) to prepare them for vesiculation. Finally, 1 ml of chemical vesicant (25 mM paraformaldehyde (PFA), 2 mM dithiothreitol (DTT) in GPMV buffer) was added to the culture dish, and the cells were incubated at 37°C for 1 hour to complete the formation of GPMVs.

2.5.1.2 Pretreatment of Gold Nanotriangle Substrate

The chip was washed with 95% ethanol and DI water, then dried with nitrogen gas. Next, the chip surface was cleaned by treating it with Ar-plasma for 10 minutes, followed by Air-plasma for 20 seconds, which also increased the hydrophilicity of the chip surface.

doi:10.6342/NTU202403291

2.5.1.3 Deposition of GPMVs and Binding of CTB

First, the PDMS was soaked in electronic-grade acetone and sonicated for 15 minutes. Then, the wells were placed in fresh acetone and left to sit for 12 hours, followed by another 15 minutes of sonication in fresh acetone. Finally, the wells were placed in an oven at 75°C for 12 hours to ensure the complete evaporation of the acetone. After plasma treatment, PDMS wells that had been cleaned with acetone were immediately attached. Then, 100 μL of GPMVs were pipetted onto the chip surface in a 1.3 cm diameter well and left to stand for 1 hour. The interaction between phospholipid headgroups and the hydrophilic chip surface was utilized to facilitate the successful rupture of vesicles and their arrangement into a two-dimensional membrane(**Figure 2-3**). Next, the sample was rinsed with PBS buffer to remove any debris.

Subsequently, 500 microliters of CTB at a concentration of 5 μg/mL were added to the system, forming a CTB solution of approximately 3.6 μg/mL to bind CTB to GM1 on the cell membrane. To enhance the rate of CTB diffusion to GM1 sites, the solution was pipetted every 15 minutes for a total of four times. The setup was then incubated at 37°C in a 5% CO_2 culture incubator for 12 hours. Finally, the excess CTB solution was rinsed off with PBS buffer.

doi:10.6342/NTU202403291

Lastly, the slides were rinsed with deionized water and dried with nitrogen gas to serve as a cover layer for the system, ensuring no bubbles were present in the solution. Before the experiment, the external surface of the substrate through which the laser passed was wiped with alcohol and deionized water.

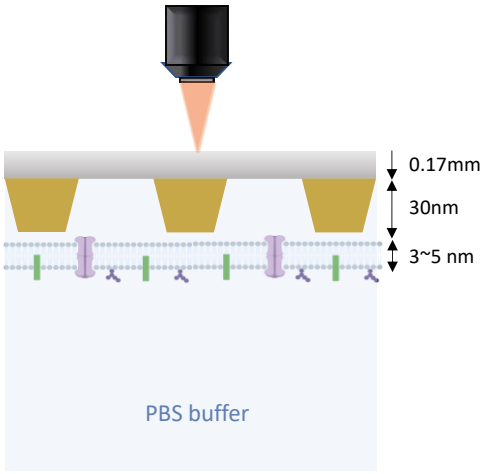

Figure 2-3 Proposed illustration of a GPMV membrane patch on the chip.

2.5.2 Formation of DOPC Supported Lipid Bilayer Platform

2.5.2.1 Lipid Preparation

First, the required amounts of DOPC and GM1 were calculated. A glass vial and a glass pipette were rinsed with chloroform and methanol. GM1 powder was poured into the glass vial, and 2400 μL of methanol was added. 100 μL of methanol were added to the original plastic bottle containing 25 mg of GM1 powder, which was then wrapped with parafilm and centrifuged for 3 minutes before pouring the solution into the glass vial.

doi:10.6342/NTU202403291

Next, 2500 μL of chloroform was added to the glass vial. The GM1 solution was then added to different glass vials according to the desired concentration. The solutions were shaken well and immediately blown with nitrogen. Finally, the solutions were vacuum dried for 12 hours, redissolved with an appropriate amount of PBS buffer, and stored in a -20°C freezer.

2.5.2.2 DOPC Lipid Extrusion Process

First, the extruder was cleaned with 95% ethanol and water. It was then assembled with a 50 nm filter. Next, 2 mg/ml DOPC containing 1 mol% GM1 was diluted with PBS buffer to achieve a 0.5 mg/ml DOPC concentration to avoid forming supported lipid multilayers. After preparation, the GM1+DOPC mixture was passed through the extruder 21 times before use.

2.5.2.3 Pretreatment of Gold Nanotriangle Substrate

The chip was washed with 95% ethanol and DI water, then dried with nitrogen gas. Next, the chip surface was cleaned by treating it with Ar-plasma for 10 minutes, followed by Air-plasma for 20 seconds, which also increased the hydrophilicity of the chip surface.

doi:10.6342/NTU202403291

2.5.2.4 Deposition of DOPC and Binding of CTB

After plasma treatment, PDMS wells that had been cleaned with acetone were immediately attached. Then, 100 μL of DOPC+GM1 was pipetted onto the chip surface in a 1.3 cm diameter well and left to stand for 1 hour. The interaction between phospholipid headgroups and the hydrophilic chip surface was utilized to facilitate the successful rupture of vesicles and their arrangement into a two-dimensional membrane(**Figure 2-4**). Next, the area surrounding the wells was rinsed with PBS buffer to minimize impurities outside the supported lipid bilayer.

Subsequently, 500 microliters of CTB at a concentration of 5 μg/mL were added to the system, forming a CTB solution of approximately 3.6 μg/mL to bind CTB to GM1 on the supported lipid bilayer. To enhance the rate of CTB diffusion to GM1 sites, the solution was pipetted every 15 minutes for a total of four times. The setup was then incubated at 37°C in a 5% CO_2 incubator for 12 hours. Finally, the excess CTB solution was rinsed off with PBS buffer.

Lastly, the slides were rinsed with deionized water and dried with nitrogen gas to serve as a cover layer for the system, ensuring no bubbles were present in the solution. Before the experiment, the external surface of the substrate through which the laser passed was wiped with alcohol and deionized water.

doi:10.6342/NTU202403291

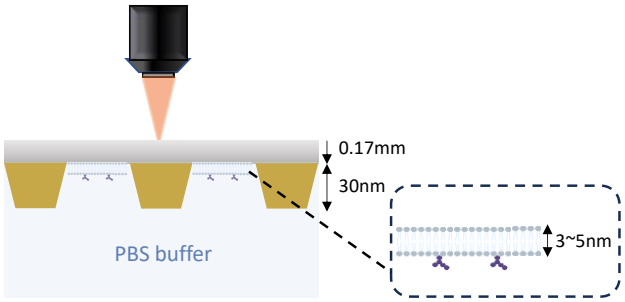

Figure 2-4 Schematic diagram of DOPC on the chip.

2.5.3 Preparation of Standard Spectra

2.5.3.1 Cholera Toxin Subunit B (CTB)

The procedure involves cleaning the surfaces of two silicon wafers by treating them with Ar-plasma for 10 minutes. Next, one wafer is treated with CTB, while the other is left untreated to serve as the background signal. Once the CTB solution has completely evaporated, leaving only CTB powder, Raman detection can be performed. The laser parameters used for both the experimental group and the control group will be kept identical to ensure that the only variable is the addition of CTB.

2.5.3.2 1,2-dioleoyl-sn-glycero-3-phosphocholine (DOPC)

The surfaces of two silicon wafers were first cleaned by treating them with Ar-plasma for 10 minutes. Meanwhile, 50 μL of DOPC and 50 μL of PBS buffer were

doi:10.6342/NTU202403291

prepared. DOPC was used for the experimental group, dissolved in PBS buffer, while PBS buffer alone was used for the control group.

Immediately after cleaning the silicon wafers, the respective samples (DOPC for the experimental group and PBS buffer for the control group) were applied, and the solvent was allowed to completely evaporate before Raman detection was performed. The laser parameters used for both the experimental and control groups were kept identical to ensure that the only variable was the addition of DOPC.

2.5.3.3 Giant Plasma Membrane Vesicles (GPMVs)

Due to the complex composition of GPMVs, overlapping characteristic peaks are often exhibited in spectra. To obtain more reliable spectra, both n-type and p-type silicon wafers were used as substrates for testing, following identical experimental procedures. First, GPMVs were obtained using the vesiculation as previously described. Containers for centrifuging GPMVs were then prepared by mixing 50 mg of agarose with 8 ml of DI water, heating the mixture in a microwave on medium-high for 1 minute, and adding approximately 300 µl of the mixture to a 2 ml centrifuge tube. Next, 1000 µl of the vesicle suspension was added to a tube, which was then placed in ice water and allowed to stand for 20 minutes to strengthen the vesicles and prevent rupture during centrifugation. The

doi:10.6342/NTU202403291

centrifuge was cooled to 10°C before centrifuging the vesicle suspension at 100 rcf for 10 minutes. After centrifugation, 900 μl of the supernatant was carefully removed, leaving behind 100 μl of concentrated vesicles, from which 50 μl was taken as the sample. Finally, 50 μl of GPMVs and 50 μl of GPMV buffer were separately deposited onto the surfaces of two identical silicon wafers and allowed to dry before Raman detection.

Chapter 3 Result and Discussion

3.1 Standard Spectra of Biomolecules on a Silicon Wafer

3.1.1 Cholera Toxin Subunit B (CTB)

Before testing our detection system, we must first understand the standard spectra of all substances in the system to analyze the data effectively. Silicon wafers are chosen as the substrate because the characteristic peak is simple and does not overlap with most of the biomolecule characteristic peaks. In the wavenumber range we are analyzing, only the wavenumber range from 900 to 1000 shows significant signals. Thus, the Raman peaks of our target substances are less interfered.

Two silicon wafers were treated with Ar-plasma for 10 minutes. Then, CTB was added on one wafer, while the other was used to obtain the background signal. Once the

doi:10.6342/NTU202403291

CTB solution has fully evaporated, leaving only CTB powder, Raman detection was performed. **Figure 3-2** shows the spetra obtained under two sets of laser parameters.

After obtaining the raw spectra, a Matlab code was used for initial background removal. The data was then normalized to eliminate the effects of substrate differences. Finally, by subtracting the spectrum of the pure silicon wafer from the CTB-treated group, we obtained the standard spectrum of the target substance.

To demonstrate that the characteristic peaks of CTB we obtained are reliable, it is necessary to compare them with the CTB Raman spectra documented in the literature.[3, 4]. However, since there is no reported CTB Raman spectra, we compared the spectra based on the Raman spectra of the amino acid sequences related to CTB. CTB is composed of a sequence of 103 amino acids[3](refer to **Figure 3-1**), so we compared the spectrum with the spectra of the most abundant 7 amino acids in the CTB sequence.

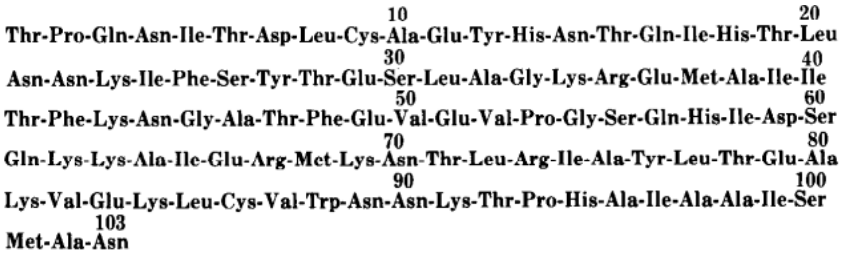

Figure 3-1 The amino acid sequence of cholera toxin B subunit (CTB)[3].

doi:10.6342/NTU202403291

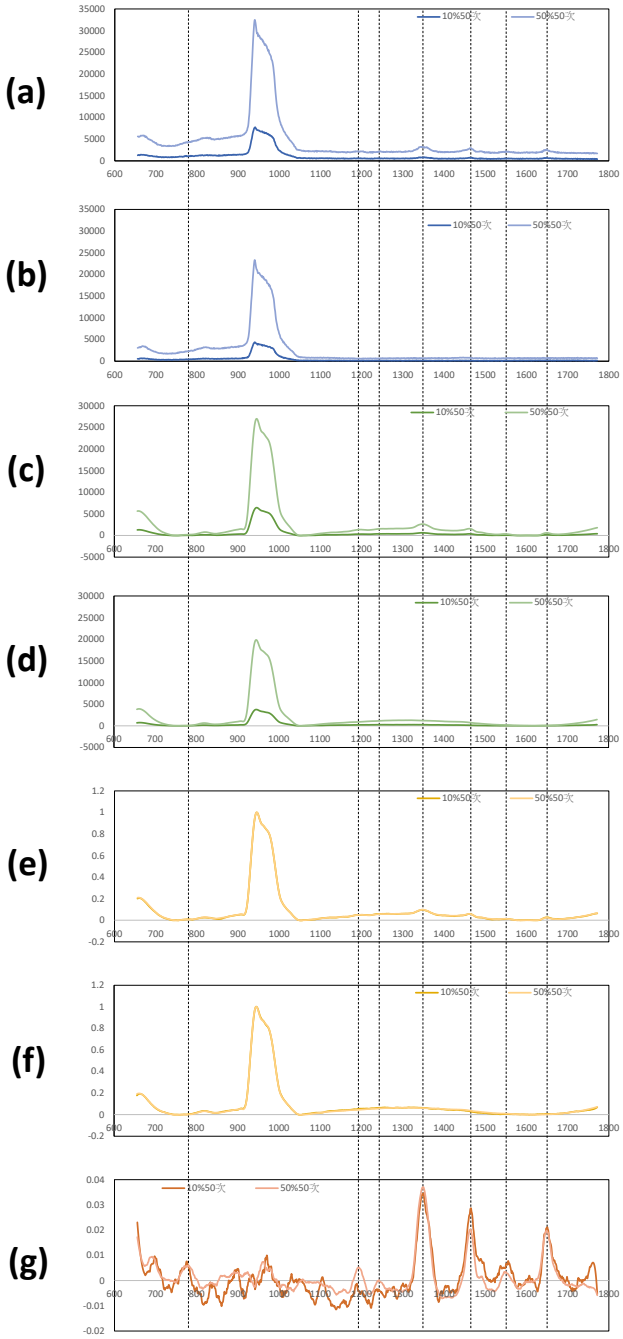

Figure 3-2 Process to obtain standard spectrum of CTB on a silicon wafer. (a)(b) The spectra of (CTB + Si) and Si before background removal. (c)(d) The spectra of (CTB + Si) and Si after background removal using a 5th-degree polynomial. (e)(f) The spectra of (CTB + Si) and Si after background removal using a 5th-degree polynomial, followed by

doi:10.6342/NTU202403291

normalization at wavenumber 946 cm^{-1}. (g) The spectrum of CTB obtained by subtracting the spectrum in (f) from the one in (e).

We consulted two articles to verify the accuracy of CTB characteristic peaks. **Figure 3-3** shows the spectra of various amino acids while solutions of amino acids were dried on the aluminum-coated slides.

Figure 3-3 compares the characteristic peaks we obtained with the spectra of the top seven abundant amino acids in CTB. After comparing characteristic peaks, we found matches for all peaks except at wavenumber 1650 cm^{-1}. Because the secondary structure of CTB is primarily β-sheet, we believe that the wavenumber 1650 cm^{-1} corresponds to the secondary structure of the amide I bond, which is probably why it does not match the primary structure of amino acids.

doi:10.6342/NTU202403291

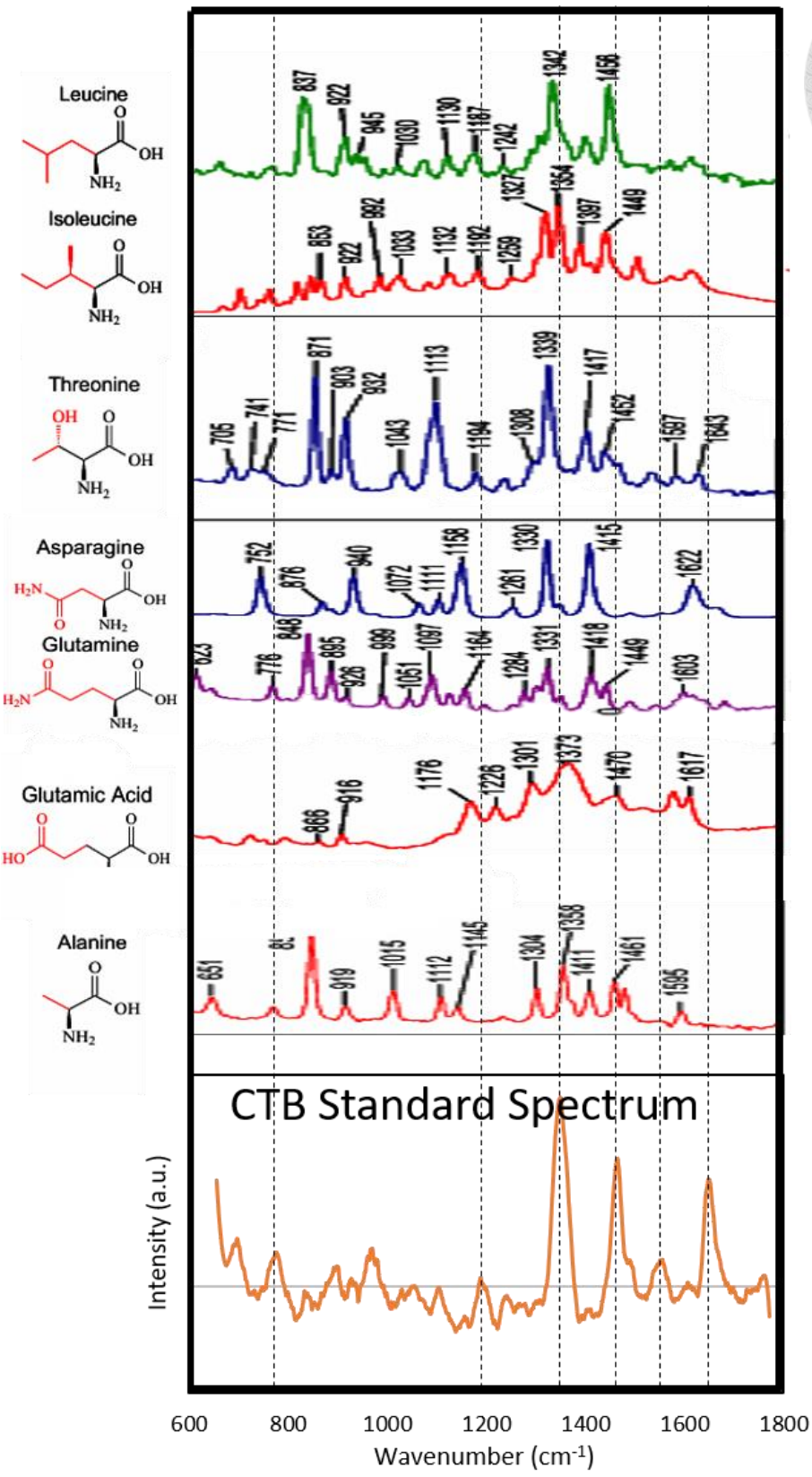

Figure 3-3 CTB standard spectrum was compared with the amino acid spectra from the

doi:10.6342/NTU202403291

literature[4].

Table 3-1 Raman peak information of amino acids for CTB.

Wavenumber(cm^{-1})	Assignment	reference
772	Ala , Gln , Ile	[4]、[5]、[6]
1190	Thr , Gln , Ile	[4]、[5]、[6]
1345	Ala , Glu , Gln , Asn , Ser , Ile , Leu , Lys , His	[4]、[5]、[6]
1462	Ala , Glu , Ser , Thr , Leu , Pro , Lys , Glu , Ile	[4]、[5]、[6]
1550	Gln , Thr , Pro	[4]、[5]、[6]
1650	Amide I	[7]、[8]

3.1.2 1,2-dioleoyl-sn-glycero-3-phosphocholine (DOPC)

For the DOPC analysis, we employed laser intensities of 10% and 50%, accumulating data over 50 times for each setting. **Figure 3-4** demonstrates that the spectra obtained under both laser treatments are consistent. **Figure 3-5** also shows that the spectra of our standard sample closely match those in the literature in terms of both characteristic peak location and shape.

doi:10.6342/NTU202403291

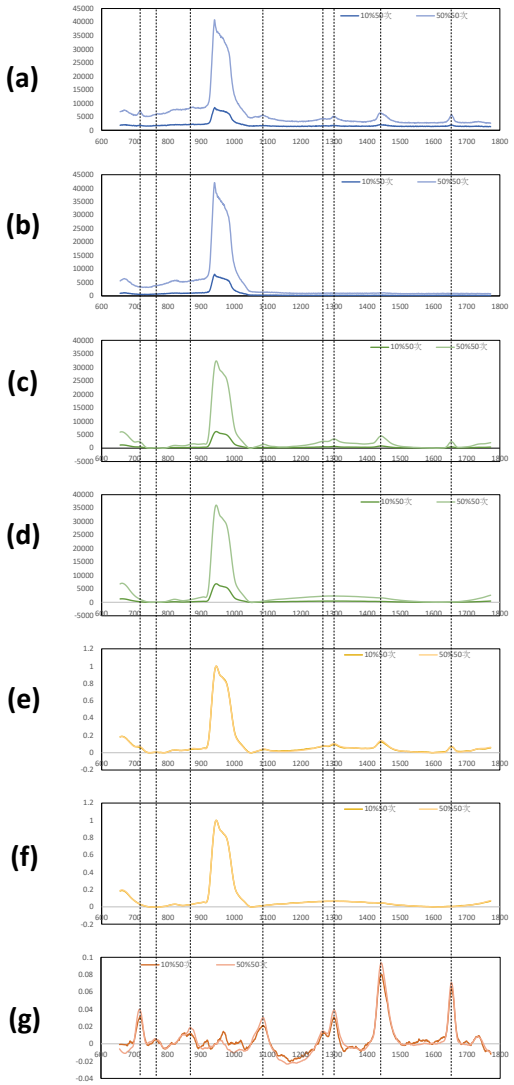

Figure 3-4 Process to obtain standard spectrum of DOPC on silicon wafer. (a)(b) The spectra of (CTB + Si) and Si before background removal. (c)(d) The spectra of (DOPC+ Si) and Si after background removal using a 5th-degree polynomial. (e)(f) The spectra of (DOPC+ Si) and Si after background removal using a 5th-degree polynomial, followed by normalization at wavenumber 946 cm^{-1}. (g) The spectrum of DOPC obtained by subtracting the spectrum in (f) from the one in (e).

doi:10.6342/NTU202403291

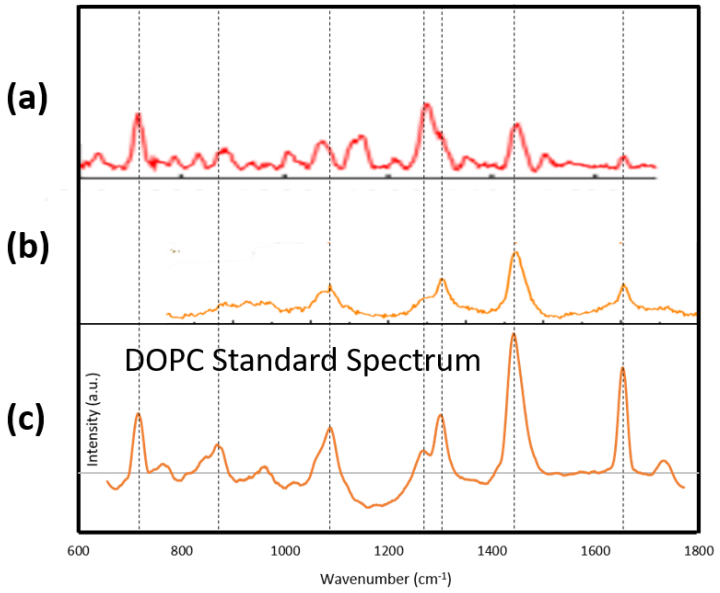

Figure 3-5 (a) The SERS spectrum of the DOPC supported lipid bilayers[9] (b) Identification of the Raman peaks measured on the DOPC supported lipid bilayers[10] (c) Dried DOPC standard spectrum on a silicon wafer.

3.1.3 Giant Plasma Membrane Vesicles (GPMVs)

Due to the properties of the substrates, the group in **Figure 3-6** was focused 5 μm above the surface of the silicon wafer. This adjustment ensured proper focus on the GPMV vesicle.

The cell membrane is composed roughly of 40-60% phospholipids, 20-25% cholesterol, 30-50% proteins, 5% glycolipids, and 2-10% carbohydrates. Therefore, we compared our measured GPMV vesicle standard spectra with several references. From

doi:10.6342/NTU202403291

the **Figure 3-7**, it can be observed that our spectra correspond to the characteristic peaks of proteins and lipids identified in the literature[11-14].

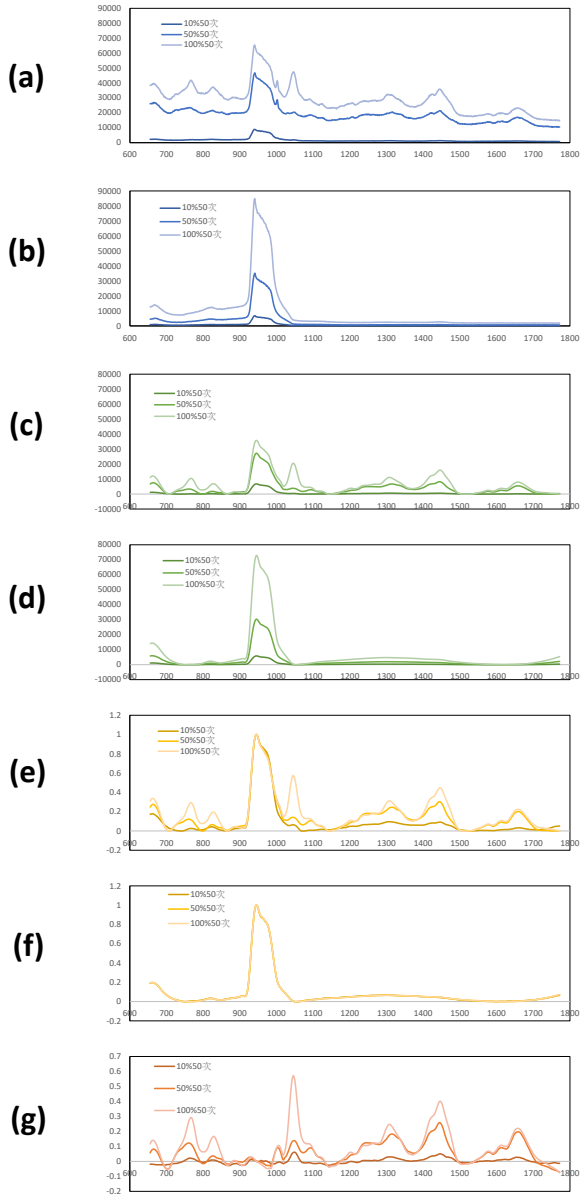

Figure 3-6 Process to obtain standard spectrum of GPMV on silicon wafer. (a)(b) The spectra of (GPMV+ Si) and Si before background removal. (c)(d) The spectra of (GPMV+ Si) and Si after background removal using a 5th-degree polynomial. (e)(f) The spectra of

doi:10.6342/NTU202403291

(GPMV+ Si) and Si after background removal using a 5th-degree polynomial, followed by normalization at wavenumber 946 cm^{-1}. (g) The spectrum of GPMV obtained by subtracting the spectrum in (f) from the one in (e).

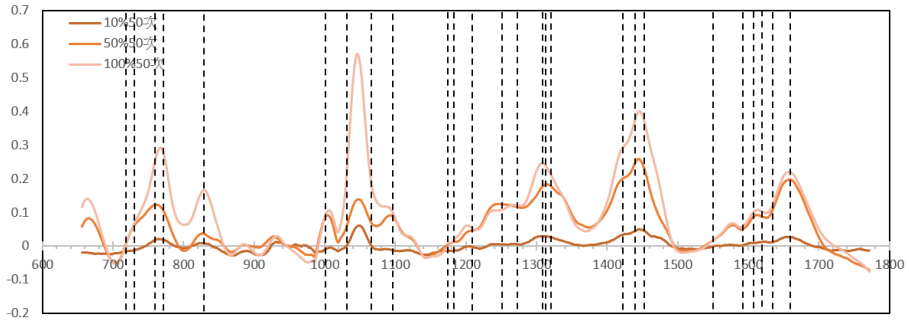

Figure 3-7 Comparison of the standard spectrum of GPMV vesicles with the characteristic peaks of various substances in the **Table 3-2**.

doi:10.6342/NTU202403291

Table 3-2 Raman peak information of substances in the cell membrane.

Wavenumber(cm^{-1})	Assignment	reference
719	phospholipid head	[11-14]
727	C-C stretch in proline	[11-14]
759	Trp	[11-14]
773	phosphatidylinositol	[11-14]
828	Tyr , v_s (PO_2^-)	[11-14]
840~870	glycolipid	[11-14]
1001	Phe	[11-14]
1032	Phe	[11-14]
1065	v_s(C-C) , v_s(C-N)	[11-14]
1097	v_s(PO_2^-) , v_s(CO-C-O)	[11-14]
1175	Tyr , Phe	[11-14]
1182	His	[11-14]
1208	Tyr , Phe , Trp	[11-14]
1254,1266	lipids	[11-14]
1220~1280	Amide III	[11-14]
1308,1313	lipids	[11-14]
1320	Amide III	[11-14]
1423	CH_2 deformation	[11-14]
1440~1455	Saturated lipids	[11-14]
1554	Amide II, Trp	[11-14]
1590	v C=C, Phe, Trp, Tyr	[11-14]
1607,1620	Tyr , Trp , Phe	[11-14]
1636	v C=O, Amide I	[11-14]
1660	Amide I	[11-14]

3.2 Fabricating the Chip for Signal Enhancement and Identifying the Appropriate Laser Operating Conditions

3.2.1 Improvement of the Chip's Capability for Signal Enhancement

doi:10.6342/NTU202403291

3.2.1.1 Impact of Different Plasma Conditions

To find the optimal parameters for fabricating the chip, we tested several different plasma conditions. Method one involved spin coating followed directly by metal deposition. This approach resulted in fragmented gold triangle structures and almost no enhancement of CTB signals on the chip. In method two, we applied the oxygen plasma to the sample to increase the distance between microparticles, hoping to bring the gold triangle vertices closer together. However, SEM images showed minimal improvement, and the CTB spectra still did not exhibit significant characteristic peaks.

Methods three, four, and five built upon the previous methods by adding a substrate cleaning step. We believed that an unclean substrate would result in the poor adhesion of gold triangles, leading to poor signal enhancement. The CTB spectra from these three methods did show consistent characteristic peaks across different locations, with method four being the most effective. Method six provided an even more thorough cleaning would yield better results. However, the CTB spectra showed less pronounced characteristic peaks, indicating that over-cleaning might be detrimental. Therefore, we ultimately chose to use method four for fabricating the chip.

doi:10.6342/NTU202403291

By improving the chip fabrication process from method 2 to method 4, we learned that the distance between adjacent gold nanotriangle vertices needs to be close enough to enhance the local electric field. From the pre-improvement SEM images, we observed that the distance between the vertices of the gold nanotriangles was about 80 nm. According to the literature[10], this distance is too large. Through testing various conditions, we found that the system achieved a distance of approximately 30 nm between the vertices of the gold nanotriangles without O_2-plasma treatment. Another important point is that if the gaps between the microspheres are not clean enough before metal deposition, it can severely affect the structure of the gold nanotriangles. Therefore, we added an additional Ar-plasma cleaning step for 20 minutes before metal deposition to clean the surface.

Finally, the Raman spectra of CTB showed that, under the same y-axis scale, the improved samples exhibited significantly enhanced characteristic peaks, and the results were consistent across different positions on the chip. In conclusion, both the SEM images and the Raman spectra of CTB demonstrate that the signal enhancement of our chip has indeed improved.

Table 3-3 The actual appearance of the surface under different chip processing parameters

doi:10.6342/NTU202403291

was observed, and signal enhancement effects were tested at three different positions on the chip(denoted as d1, d2, d3).

	Method 1	Method 2	Method 3	Method 4	Method 5	Method 6
Adjusting the distance between polystyrene microspheres	No treatment	O_2-plasma 100s	Ar-plasma 20min	No treatment	O_2-plasma 100s	Ar-plasma 20min
Cleaning the chip before metal deposition	No treatment	No treatment	No treatment	Ar-plasma 20min	Ar-plasma 20min	Ar-plasma 20min
SEM image	Top view	Top view	Top view	Top view	Top view	Top view
						
Bright-field image in PBS buffer	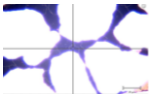	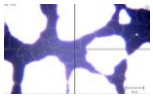	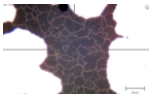	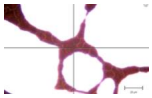		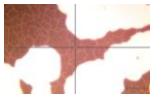
Spectrum (CTB on a chip)	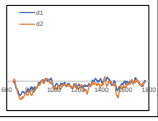	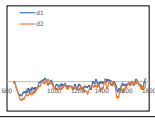	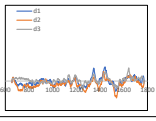	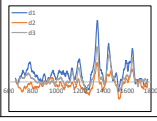	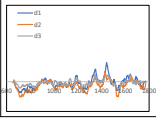	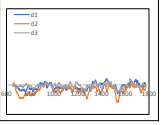

3.2.1.2 Reason to Test Polystyrene Microparticles from Different Brands

Considering that a cleaner chip surface makes it easier to create structurally complete gold triangles, we suspected that the polystyrene beads from Bang Laboratories, which contains substances besides water to help evenly disperse the polystyrene microparticles, might be the source of surface contaminants. Therefore, we also tested polystyrene beads from microParticles GmbH, which contains only polystyrene microparticles and water.

doi:10.6342/NTU202403291

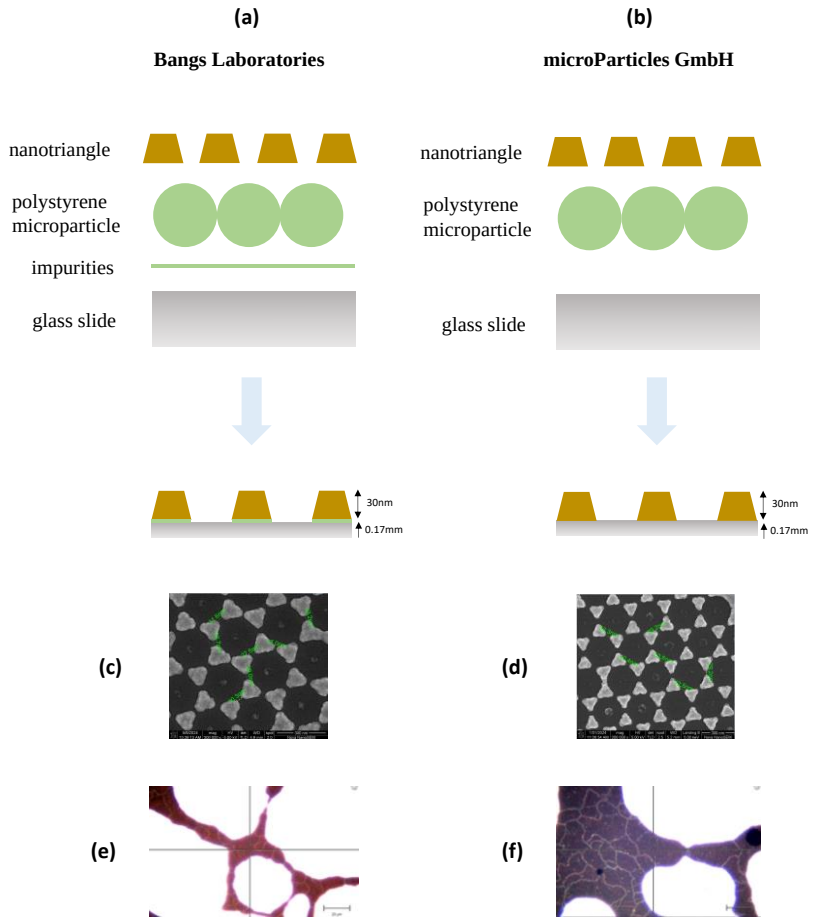

Figure 3-8 (a)(b) Schematic diagram of the chips fabricated by the polystyrene beads from Bang Laboratories and from GmbH, respectively. (c)(d) SEM images of the chip made with beads from Bang Laboratories and from GmbH, respectively. (e)(f) Bright-field images of the chip made with beads from Bang Laboratories and from GmbH, respectively. The composition of polystyrene beads from Bang Laboratories contains 89.41% DI water, 10% polystyrene microspheres, 0.5% Sodium dodecyl sulfate, and 0.09% Sodium azide. Polystyrene beads from microParticles GmbH consist of 10% polystyrene microspheres and 90% DI water.

doi:10.6342/NTU202403291

3.2.2 Deposition of a DOPC-supported Lipid Bilayer on the Chip

To ensure that DOPC lipid vesicles can uniformly deposit on the chip in our system, we tracked the process by staining DOPC lipid vesicles with Fast-Dio fluorescent dye. In **Figure 3-10** (a), it can be observed that the gray areas represent the gold triangle regions, while the black areas are the fully gold-covered regions. **Figure 3-10** (b) shows that DOPC lipid vesicles or membranes did stably adhere to the gold triangle regions after the rinsing step.

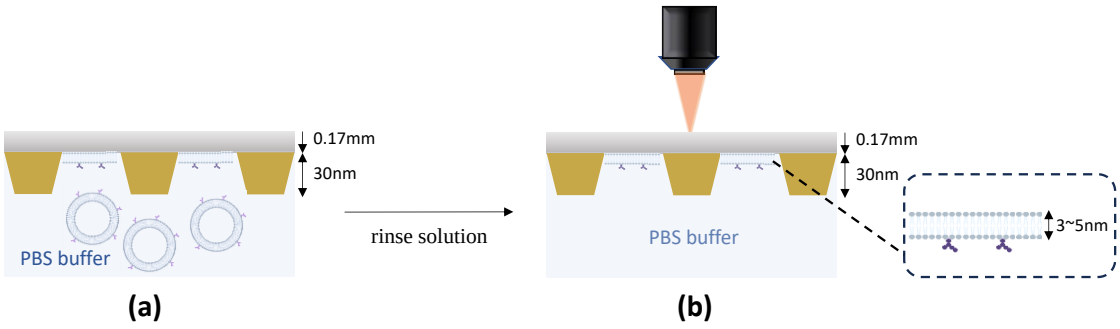

Figure 3-9 Schematic diagram of the sample (a) after the addition of DOPC lipid vesicles; (b) after the excessive DOPC lipid vesicles were washed away.

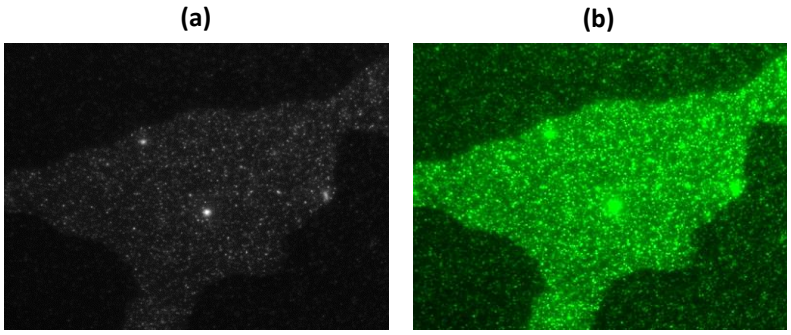

Figure 3-10 (a) Bright-field image of DOPC lipid membranes on a chip (b) Fluorescence

doi:10.6342/NTU202403291

image of DOPC lipid membranes on a chip.

3.2.3 Depositing the GPMVs on the Chip

To locate the GPMV patches in the gold triangle regions, we stained the GPMVs with Fast-Dio fluorescent dye. In **Figure 3-12** (a), the blue areas with gold lines represent the regions where the gold triangles are present. In **Figure 3-12** (b), the fluorescent image shows that a GPMV patch located within the gold triangle regions.

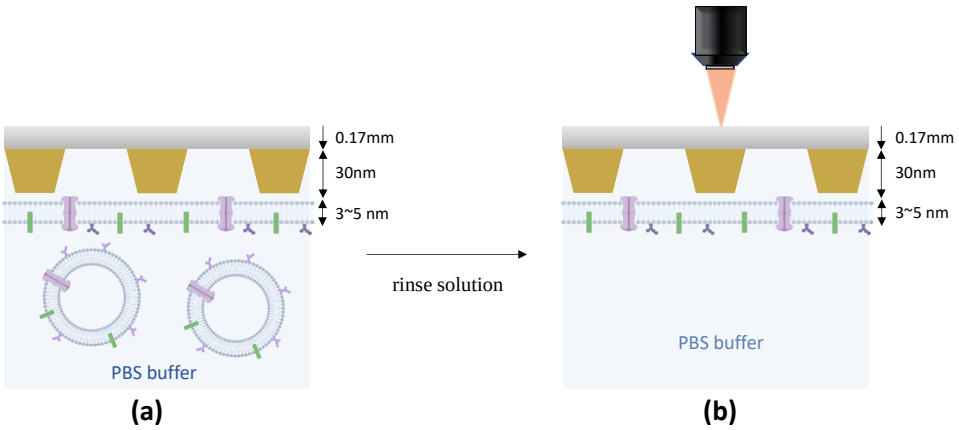

Figure 3-11 (a) Schematic diagram of the samples after the addition of GPMVs. (b) Schematic diagram of the system for Raman detection of the sample after the excessive GPMVs were washed away.

doi:10.6342/NTU202403291

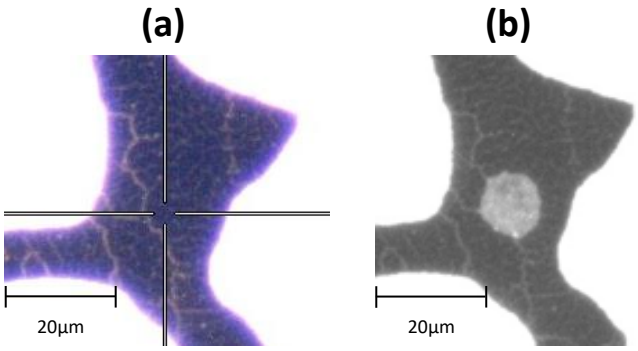

Figure 3-12 (a) Bright-field image of GPMVs on a chip (b) Fluorescence image of GPMVs on a chip.

3.2.4 Effect of Laser Intensity on Biomolecules

Since it is already known that laser may damage biomolecules, we tested the impact of three different laser intensities (10%, 1%, 0.5%) on the CTB. From **Figure 3-13** (a), it could be seen that the characteristic peak at a wavenumber of 1550 cm^{-1} showed significant changes with increasing laser accumulations, indicating structural changes in CTB. In **Figure 3-13** (b), reducing the laser intensity to 1% resulted in better consistency of the characteristic peaks; however, wavenumbers between 700-800 cm^{-1} showed characteristic peaks that were not present in the standard spectrum. Finally, in **Figure 3-13** (c), at a laser intensity of 0.5%, the characteristic peak at a wavenumber of 1442 cm^{-1} shifted with increasing laser accumulations. Given that an excessively low laser intensity would result in a low signal-to-noise ratio for Raman signals, we opted to maintain the laser intensity at 0.5% and explore other methods to address the issue of characteristic

doi:10.6342/NTU202403291

peak shifts. By observing the spectra obtained from these three laser parameters, we found that the spectral characteristic peaks at both 1% and 0.5% laser intensity had higher consistency. Therefore, we decided to use a laser intensity of 0.5% for subsequent tests.

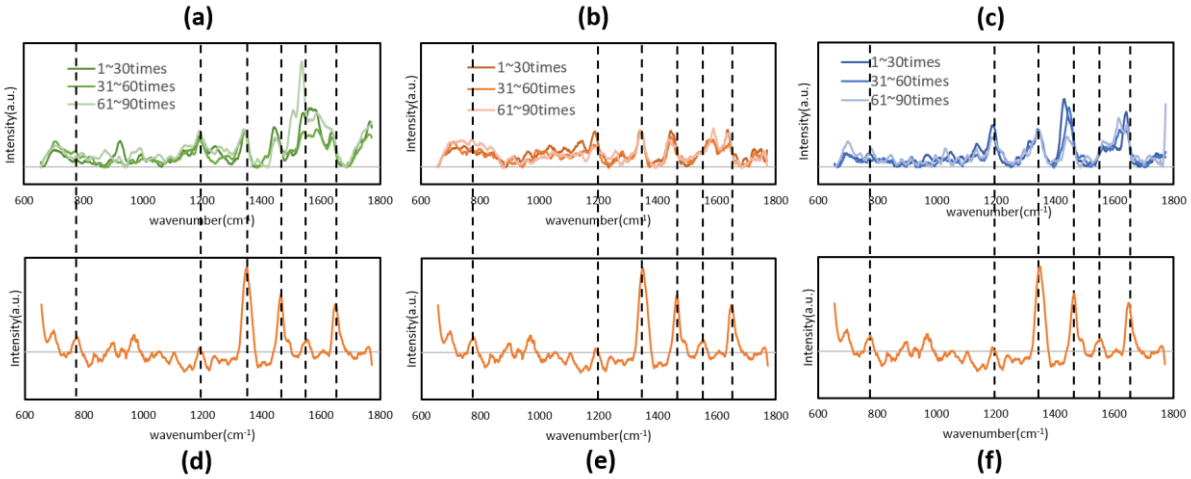

Figure 3-13 The spectral changes of CTB on the chip over time under different laser parameters were used to determine whether the structure of CTB had changed. Our method involved accumulating laser shots 90 times at the same location. The three lines in each spectrum in the top panel indicate the accumulation of spectra from the 1st to 30th shots, the 31th to 60th shots, and the 61th to 90th shots. (a) CTB spectrum obtained with 10% laser intensity; (b) CTB spectrum obtained with 1% laser intensity; (c) CTB spectrum obtained with 0.5% laser intensity (d)(e)(f) Standard spectra of CTB on a silicon wafer.

doi:10.6342/NTU202403291

3.2.5 Using Intermittent Accumulation to Reduce the Damage to Biomolecules in Our System

Here, we speculated that the shift in characteristic peaks may be due to heat accumulation in the laser region. Based on a laser intensity of 0.5%, we introduced intervals between each laser pulse to allow sufficient time for the localized area to dissipate heat, aiming to resolve the issue of peak shifts. We tested a laser interval time of 10 seconds. As shown in **Figure 3-14** (b), the positions of the CTB characteristic peaks, indicated by dashed lines, exhibited almost no shifts or shape changes with increasing laser accumulations. This suggests that our method effectively obtained consistent spectra. Therefore, we adopted the laser parameters from **Figure 3-14** (b) for subsequent experiments.

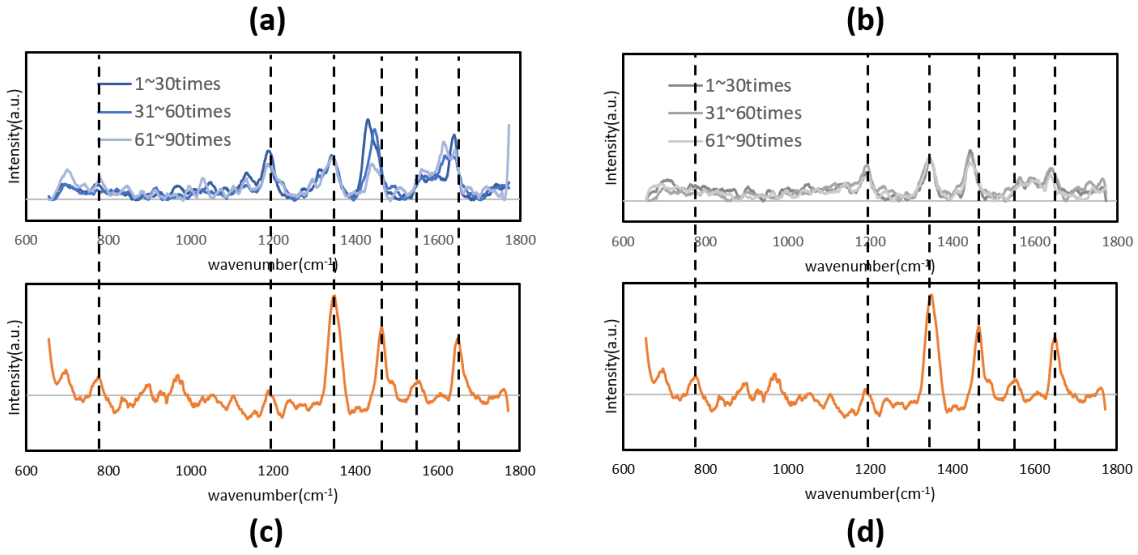

Figure 3-14 The spectral changes of CTB on the chip over time under different laser

doi:10.6342/NTU202403291

parameters with 10 second interval were used to determine whether the structure of CTB had changed. Our method involved accumulating laser shots 90 times at the same location. The three lines in each spectrum in the top panel indicate the accumulation of spectra from the 1st to 30th shots, the 31th to 60th shots, and the 61th to 90th shots. (a) CTB spectrum obtained with 0.5% laser intensity; (b) CTB spectrum obtained with 0.5% laser intensity and a 10-second interval between each laser pulse; (c)(d) Standard spectra of CTB on a silicon wafer.

3.3 Detection of DOPC Supported Lipid Bilayers on the Fabricated Chips

Since we are unsure which brand of polystyrene microparticles produces the best results for chip fabrication, we will test all of them. Therefore, each parameter tested will have two sets of results.

3.3.1 Impact of the Detection Method and Fabrication Process on the Spectral Acquisition of DOPC-Supported Lipid Bilayers

In the upside down measurements on chips treated with Ar-plasma for 10 minutes

doi:10.6342/NTU202403291

group, we adopted a method of inverting the chip to avoid interference from the solution in the Raman scattering. Additionally, we treated the chip with Ar-plasma for 10 minutes before depositing DOPC to ensure a clean surface. We also used polystyrene beads from two different brands to test the impact of varying compositions.

From **Figure 3-16**, we can see that Raman detection was performed at three different locations on both the experimental and control groups to avoid contamination at a specific location that could distort the results. The raw spectra were smoothed to remove noise, and a 5th order polynomial was used for background removal. Then, we normalized the spectra using the wavenumber 800 cm^{-1} to eliminate variations in signal enhancement between different chips. Finally, the control group spectrum was subtracted from the experimental group spectrum to complete the spectral analysis.

In the upside down measurements on chips treated with Ar-plasma for 10 minutes followed by additional air-plasma treatment for 20 seconds group, the reason for performing additional air-plasma treatment on the chip here was due to the observation that after adding DOPC, it did not spread evenly on the chip surface but forms liquid droplets instead (**Figure 3-15**). This is likely caused by the insufficient hydrophilicity of the chip surface. However, because air-plasma treatment may have an etching effect on the substrate, the treatment duration should not be too long.

doi:10.6342/NTU202403291

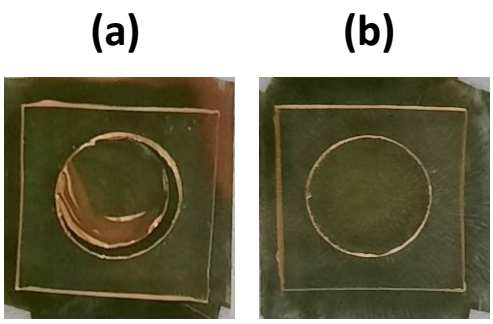

Figure 3-15 (a) Air-plasma treatment was not applied for 20 seconds before the DOPC lipid vesicle deposition (b) Air-plasma treatment was applied for 20 seconds before the DOPC lipid vesicle deposition.

In the upside up measurements on chips treated with Ar-plasma for 10 minutes followed by additional air-plasma treatment for 20 seconds group, due to the GPMV membrane patch being located above the gold nanotriangle, there's concern that if the chip is inverted, the Raman scattering from the GPMV membrane patch might be obstructed by the gold. However, when the chip is in the upside up orientation, the laser path passes through the solution, which might scatter the Raman signals. Therefore, we have fabricated a PDMS well of the same thickness as the silicon wafer, aiming to minimize the distance the laser travels through the solution as much as possible.

doi:10.6342/NTU202403291

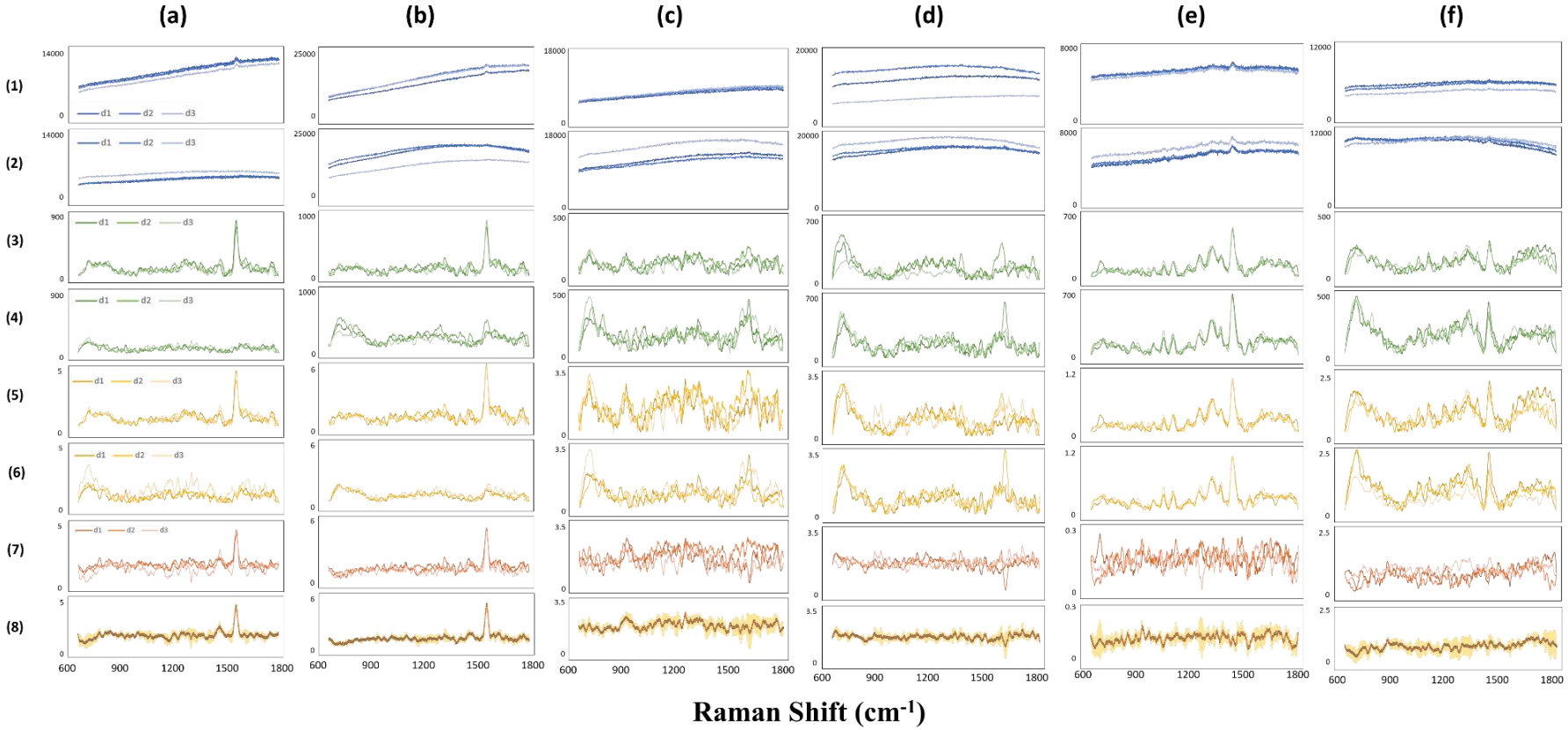

doi:10.6342/NTU202403291

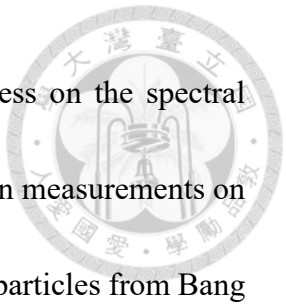

Figure 3-16 The impact of the detection platform fabrication process on the spectral acquisition of DOPC-supported lipid bilayers. (a) and (b) upside down measurements on chips treated with Ar-plasma for 10 minutes, using polystyrene microparticles from Bang Laboratories and GmbH, respectively. (c) and (d) upside down measurements on chips treated with Ar-plasma for 10 minutes followed by additional air-plasma treatment for 20 seconds, using polystyrene microparticles from Bang Laboratories and GmbH, respectively. (e) and (f) upside up measurements on chips treated with Ar-plasma for 10 minutes followed by additional air-plasma treatment for 20 seconds, using polystyrene microparticles from Bang Laboratories and GmbH, respectively. Process to obtain spectrum of DOPC with 1 mol% GM1 on chips. process to obtain spectrum of DOPC on chips. (1) and (2) the spectra of (DOPC (with GM1) + PBS buffer + chip) and (PBS buffer + chip) before background removal. (3) and (4) the spectra of (DOPC (with GM1) + PBS buffer + chip) and (PBS buffer + chip) after background removal using a 5th-degree polynomial. (5) and (6) the spectra of (DOPC (with GM1) + PBS buffer + chip) and (PBS buffer + chip) after background removal using a 5th-degree polynomial, followed by normalization at wavenumber 800 cm^{-1}. (7) the spectrum of DOPC obtained by subtracting the spectrum in (6) from the one in (5). (8) average of all spectra in (7).

doi:10.6342/NTU202403291

3.3.2 Comparison of Spectra from Different Chip Treatments

From **Figure 3-17** (a) and (b), a significant characteristic peak at a wavenumber of 1535 cm^{-1} was observed. However, this same feature was not seen in **Figure 3-17** (c) and (d). Since this characteristic peak was not associated with DOPC, we inferred that the chip surface treated with Air-plasma for 20 seconds was indeed cleaner. In **Figure 3-17** (c), it was observed that, except for the wavenumber range of 800-900 cm^{-1}, almost all the DOPC standard characteristic peaks were present. However, the Raman peaks were not very prominent. I believed this was because the standard sample consisted of multiple layers, whereas the DOPC deposited on the chip was a monolayer. Therefore, under the same light collection conditions, the standard sample could collect more Raman scattering. Although **Figure 3-17** (d) also showed some characteristic peaks corresponding to the standard spectrum, the signals were clearly less pronounced. We inferred that the GmbH chip could indeed make the chip cleaner during the preparation process, with a more complete gold nanotriangle structure. **Figure 3-17** (e) and (f) showed almost no characteristic peaks, suggesting that Raman scattering detection with the sample upside up was severely interfered with by the aqueous solution. In summary, **Figure 3-17** (c) showed the best parameters for detecting DOPC on the chip.

doi:10.6342/NTU202403291

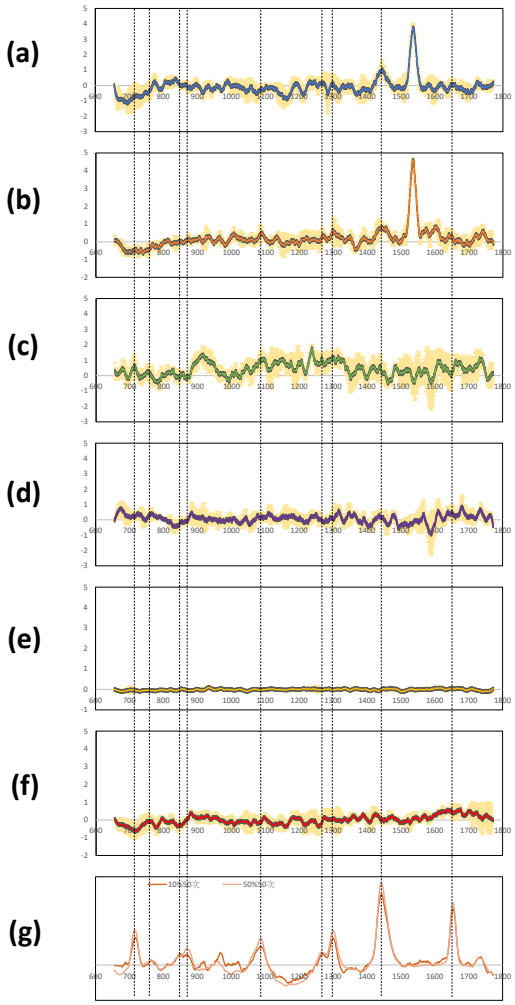

Figure 3-17 Raman spectra of DOPC on chips obtained with different process parameters (a) upside down with GmbH chip treated with 10 minutes Ar-plasma before adding DOPC; (b) upside down with Bang laboratory chip treated with 10 minutes Ar-plasma before adding DOPC; (c) upside down with GmbH chip treated with 10 minute Ar-plasma + 20 second air-plasma before adding DOPC; (d) upside down with Bang laboratory chip treated with 10 minute Ar-plasma + 20 second air-plasma before adding DOPC; (e) upside up with GmbH chip treated with 10 minute Ar-plasma + 20 second air-plasma before

doi:10.6342/NTU202403291

adding DOPC; (f) upside up with Bang laboratory chip treated with 10 minute Ar-plasma + 20 second air-plasma before adding DOPC; (g) standard spectrum of DOPC.

3.4 Detection of the Cell Membrane from GPMVs on the Fabricated Chips

3.4.1 Impact of the Detection Method and Fabrication Process on the Spectral Acquisition of the GPMV Membrane Patch

Our native cell membrane is chemically vesiculated using Hela cells, utilizing the hydrophilic interactions between cell membrane headgroups and the chip surface to break vesicles and form a supported cell membrane. Unlike DOPC, native cell membranes contain cholesterol, which could prevent easy disruption[15]. The diameter of the GPMV patch is approximately 10-20 μm, which is much larger in scale than the gold nanotriangle. Additionally, cholesterol helps maintain a certain tension in the cell membrane, preventing it from collapsing. This is why we hypothesize that GPMV patches can span across the gold nanotriangle (refer to **Figure 3-18**). Additionally, cholesterol enhances membrane stability, reducing liquefaction at high temperatures and solidification at low temperatures, contributing to membrane resilience during laser processes.

doi:10.6342/NTU202403291

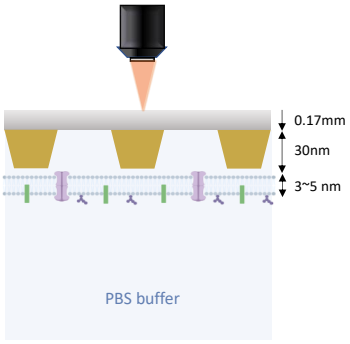

Figure 3-18 Proposed illustration of a GPMV membrane patch on the chip.

The idea of upside up measurements on chips originated from the concern that with the GPMV membrane patch located above the gold nanotriangle, if the chip is inverted, the Raman scattering from the GPMV membrane patch might be obstructed by the gold (refer to **Figure 3-19**). However, when the chip is in the upside up orientation, the laser path passes through the solution. The Raman signals might scattered by the solution. Therefore, we have fabricated a PDMS well of the same thickness as the silicon wafer, aiming to minimize the distance the laser travels through the solution as much as possible.

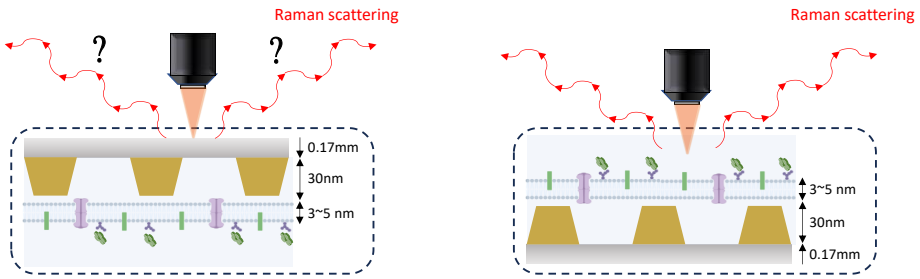

Figure 3-19 Schematic diagram of the upside down (left) and upside up measurements (right).

doi:10.6342/NTU202403291

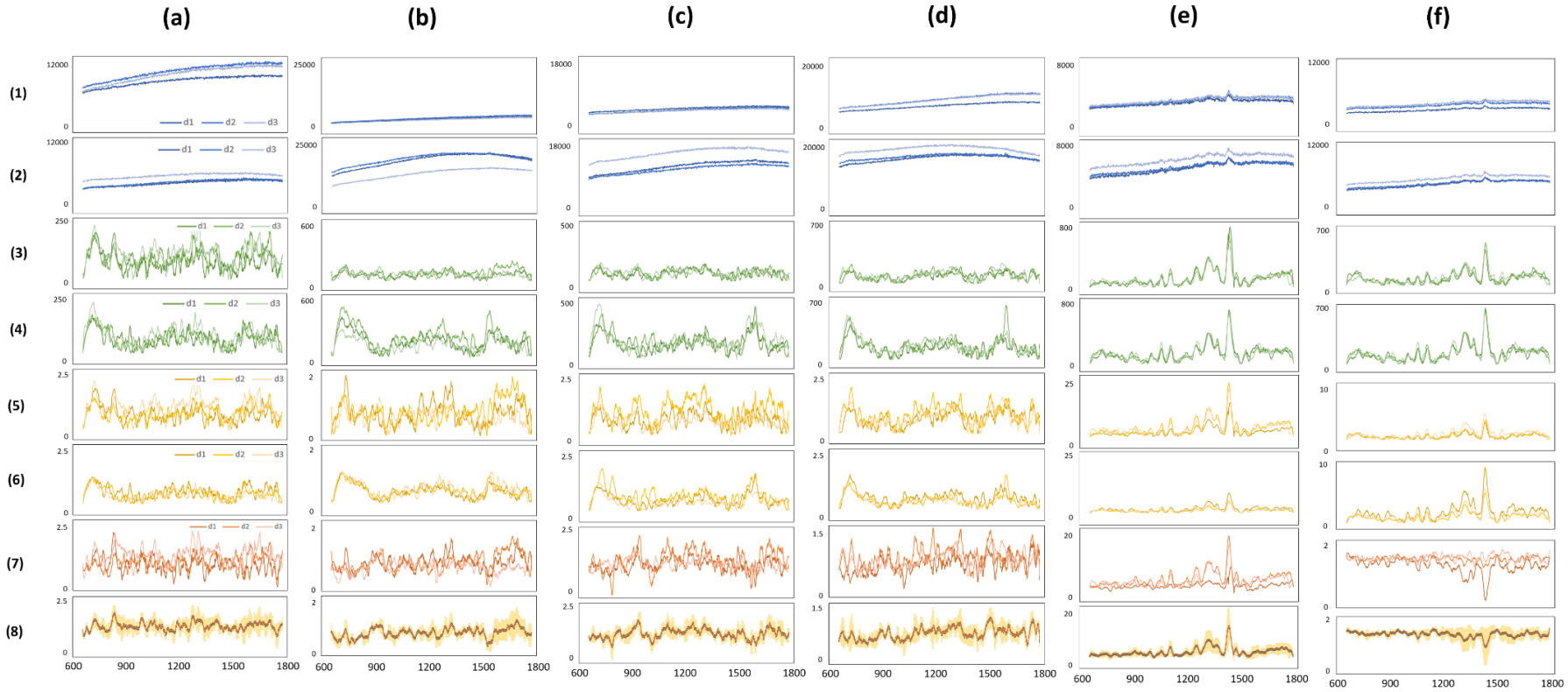

doi:10.6342/NTU202403291

Figure 3- 20 The impact of the detection platform fabrication process on the spectral acquisition of the GPMV membrane patch. (a) and (b) upside down measurements on chips treated with Ar-plasma for 10 minutes, using polystyrene microparticles from Bang Laboratories and GmbH, respectively. (c) and (d) upside down measurements on chips treated with Ar-plasma for 10 minutes followed by additional air-plasma treatment for 20 seconds, using polystyrene microparticles from Bang Laboratories and GmbH, respectively. (e) and (f) upside up measurements on chips treated with Ar-plasma for 10 minutes followed by additional air-plasma treatment for 20 seconds, using polystyrene microparticles from Bang Laboratories and GmbH, respectively. process to obtain spectrum of GPMV on chips. (1)(2) The spectra of (GPMV + PBS buffer + chip) and (PBS buffer + chip) before background removal. (3)(4) The spectra of (GPMV + PBS buffer + chip) and (PBS buffer + chip) after background removal using a 5th-degree polynomial. (5)(6) The spectra of (GPMV + PBS buffer + chip) and (PBS buffer + chip) after background removal using a 5th-degree polynomial, followed by normalization at wavenumber 700 cm^{-1}. (7) The spectrum of GPMV obtained by subtracting the spectrum in (6) from the one in (5). (8) average of all spectra in (7).

3.4.2 Comparison of Different Chip Treatments

doi:10.6342/NTU202403291

Figure 3-21 (a) and (b) compared to the GPMV standard spectrum revealed that the characteristic peaks were not consistent. Based on our previous experience, we believed that the chip surface treated with Air-plasma for 20 seconds was cleaner. However, as shown in **Figure 3-21** (c) and (d), the spectral trends did not improve significantly. Next, we suspected that the gold nanotriangles might be obstructing the Raman scattering of the cell membrane, so we placed the chip upside up on the stage. Although some characteristic peaks were observed in **Figure 3-21** (e) and (f), they were clearly inconsistent with the GPMV standard spectrum. Therefore, we concluded that the detected Raman peaks might be signals from the substrate. In summary, in the current tests, our chip could not detect the GPMV signal.

doi:10.6342/NTU202403291

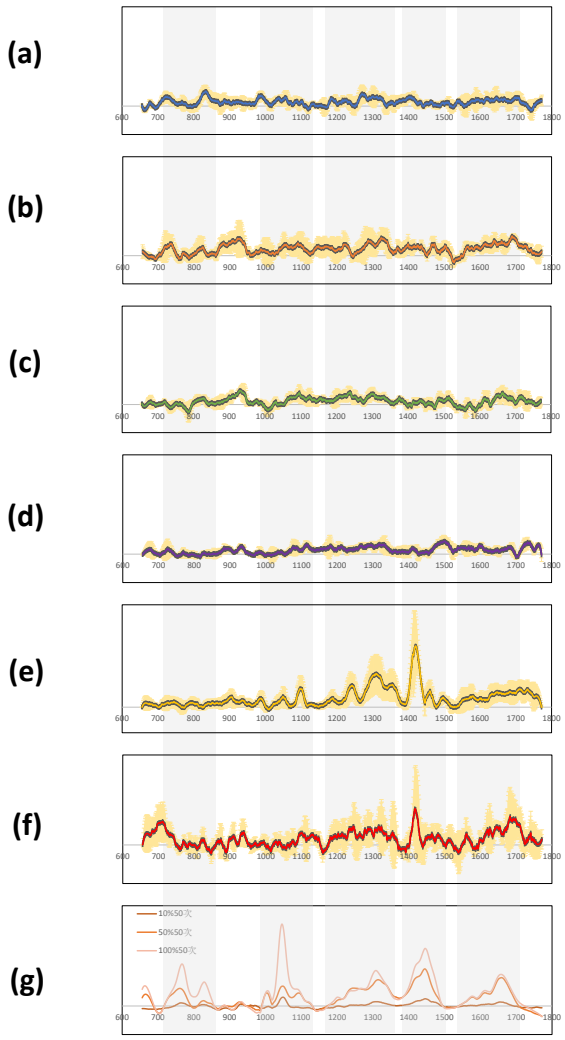

Figure 3-21 Raman spectra of GPMV patch on chips obtained with different process parameters (a) upside down with GmbH chip treated with 10 minutes Ar-plasma before adding GPMV; (b) upside down with Bang laboratory chip treated with 10 minutes Ar-plasma before adding GPMV; (c) upside down with GmbH chip treated with 10 minute Ar-plasma + 20 second air-plasma before adding GPMV; (d) upside down with Bang laboratory chip treated with 10 minute Ar-plasma + 20 second air-plasma before adding GPMV; (e) upside up with GmbH chip treated with 10 minute Ar-plasma + 20 second air-

doi:10.6342/NTU202403291

plasma before adding GPMV; (f) upside up with Bang laboratory chip treated with 10 minute Ar-plasma + 20 second air-plasma before adding GPMV; (g) standard spectrum of GPMV.

3.5 Detection of CTB Directly on the Fabricated Chips

3.5.1 Impact of the Detection Method and Fabrication Process on the Spectrum Acquisition of CTB

CTB has a molecular diameter of approximately 3.5 nm, and the distance between adjacent gold nanotriangle vertices is about 30 nm. Therefore, CTB molecules can enter the gaps between the gold nanotriangles.(refer to **Figure 3-22**).

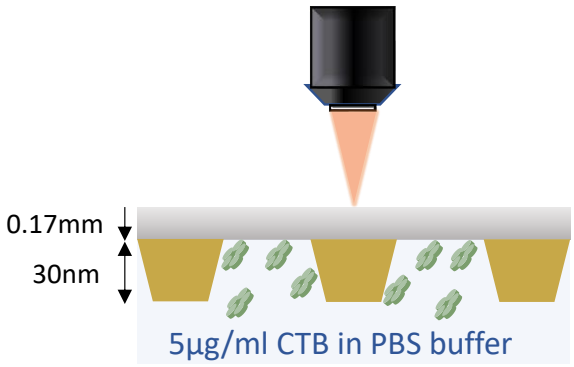

Figure 3-22 Schematic diagram of cholera toxin subunit B on the chip.

I believe there are two important purposes for detecting CTB on the chip. First,

doi:10.6342/NTU202403291

because the characteristic peaks of the same substance can show slight differences between non-enhanced and enhanced substrates, it is necessary to create a standard spectrum of CTB on the chip, even if we already have the standard spectrum of CTB on a silicon wafer. This ensures more accurate comparison results when analyzing CTB on the membrane in the future. Second, since CTB signals are the easiest for us to detect, they can serve as a benchmark for determining the quality of the chip.

doi:10.6342/NTU202403291

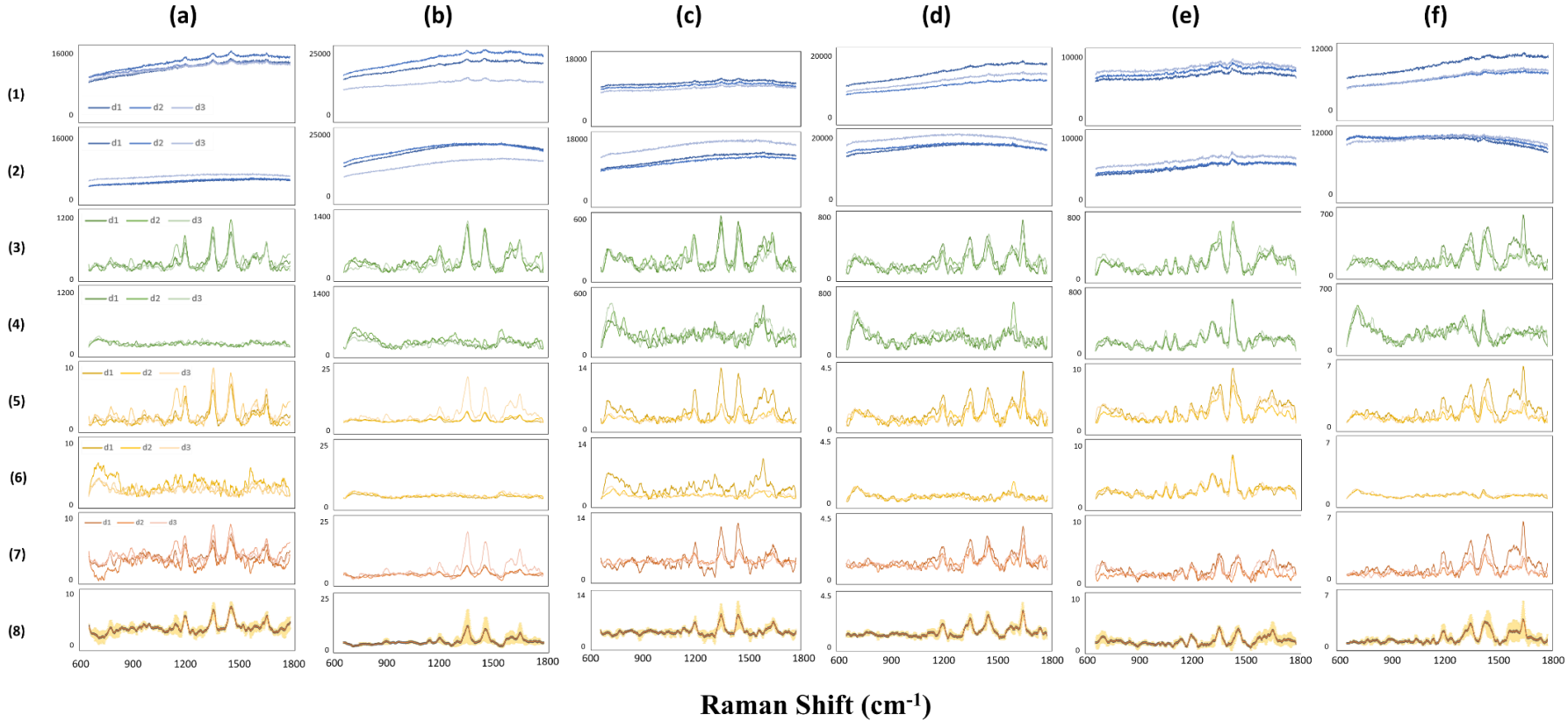

doi:10.6342/NTU202403291

Figure 3-23 The impact of the detection platform fabrication process on the spectrum acquisition of CTB directly on the chip. (a) and (b) upside down measurements on chips treated with Ar-plasma for 10 minutes, using polystyrene microparticles from Bang Laboratories and GmbH, respectively. (c) and (d) upside down measurements on chips treated with Ar-plasma for 10 minutes followed by additional air-plasma treatment for 20 seconds, using polystyrene microparticles from Bang Laboratories and GmbH, respectively. (e) and (f) upside up measurements on chips treated with Ar-plasma for 10 minutes followed by additional air-plasma treatment for 20 seconds, using polystyrene microparticles from Bang Laboratories and GmbH, respectively. process to obtain spectrum of CTB on chips. (1)(2) the spectra of (CTB + PBS buffer + chip) and (PBS buffer + chip) before background removal. (3)(4) the spectra of (CTB + PBS buffer + chip) and (PBS buffer + chip) after background removal using a 5th-degree polynomial. (5)(6) the spectra of (CTB + PBS buffer + chip) and (PBS buffer + chip) after background removal using a 5th-degree polynomial, followed by normalization at wavenumber 1000 cm^{-1}. (7) The spectrum of CTB obtained by subtracting the spectrum in (6) from the one in (5). (8) average of all spectra in (7).

3.5.2 Comparison of Different Chip Treatments

doi:10.6342/NTU202403291

By comparing the test results of all groups with the standard spectrum of CTB, we observed that apart from the characteristic peaks at wavenumbers 772 cm^{-1}, all other characteristic peaks matched the standard spectrum across all groups. As previously mentioned, the spectra obtained from enhanced substrates and non-enhanced substrates might have slight differences, which is evident in the characteristic peaks between wavenumbers 1400 cm^{-1} and 1500 cm^{-1}. However, the overall spectral trend is very similar across different substrates, suggesting the reliability of the CTB spectrum on the chip.

Additionally, figures (g) and (h) in **Figure 3-24** represent the same standard spectrum, but when the y-axis scale of (g) was adjusted to match that of the other spectra, the signals were nearly invisible. Therefore, two standard spectra with different scales are presented. It is worth noting that the laser parameters for CTB on the chip used a laser intensity of 0.5% with 150 accumulations, while CTB on the silicon wafer used a laser intensity of 10% and 50%, with 50 accumulations. The laser used to create the standard spectrum was significantly stronger, yet almost no characteristic peaks were observed, further proving that our chip indeed enhances the signal. Simultaneously, we calculated the enhancement factor to be approximately 192 using the formula (3-1).

doi:10.6342/NTU202403291

$$\mathrm{EF} = \left(\frac{I_{\mathrm{SERS}}}{I_{\mathrm{normal}}}\right)\left(\frac{N_{\mathrm{normal}}}{N_{\mathrm{SERS}}}\right) \quad (3\text{-}1)$$

where

I_{SERS} = the intensity of the Raman signal with enhancement.

I_{normal} = the intensity of the Raman signal without enhancement.

N_{SERS} = the number of molecules contributing to the Raman signal in the SERS measurement.

N_{normal} = the number of molecules contributing to the Raman signal in the normal Raman measurement.

doi:10.6342/NTU202403291

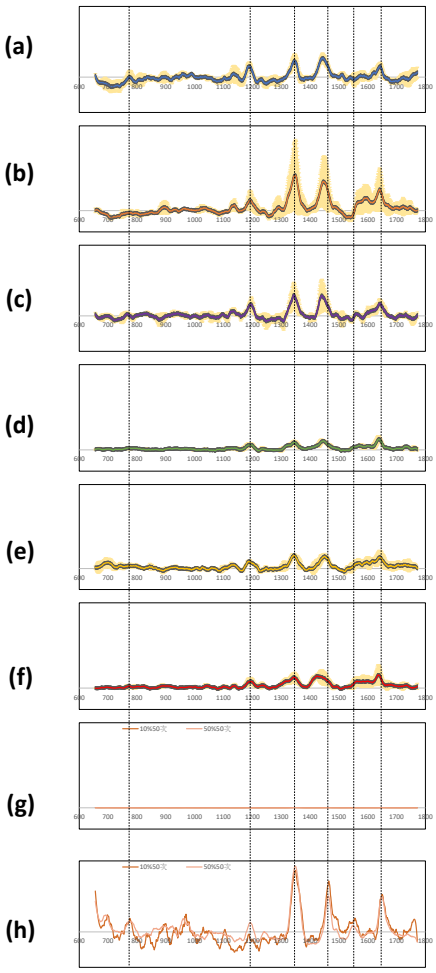

Figure 3-24 Raman spectra of CTB on chips obtained with different process parameters (a) upside down with GmbH chip treated with 10 minutes Ar-plasma before adding CTB; (b) upside down with Bang laboratory chip treated with 10 minutes Ar-plasma before adding CTB; (c) upside down with GmbH chip treated with 10 minute Ar-plasma + 20 second air-plasma before adding CTB; (d) upside down with Bang laboratory chip treated with 10 minute Ar-plasma + 20 second air-plasma before adding CTB; (e) upside up with GmbH chip treated with 10 minutes Ar-plasma before adding CTB; (f) upside up with

doi:10.6342/NTU202403291

Bang laboratory chip treated with 10 minutes Ar-plasma before adding CTB; (g) standard CTB spectrum; (h) standard CTB spectrum with adjusted y-axis scale.

3.6 Performing CTB Detection on a Fabricated Chip with a DOPC-Supported Lipid Bilayer

3.6.1 Impact of the Detection Method and Fabrication Process on the Spectrum Acquisition of CTB on the Chip with a DOPC-Supported Lipid Bilayer

Here, we used a DOPC-supported lipid bilayer as the detection platform and incorporated 1 mol% GM1 to bind CTB. We employed six different sample preparation methods to understand the impact of air-plasma treatment and chip placement on the detection results.

doi:10.6342/NTU202403291

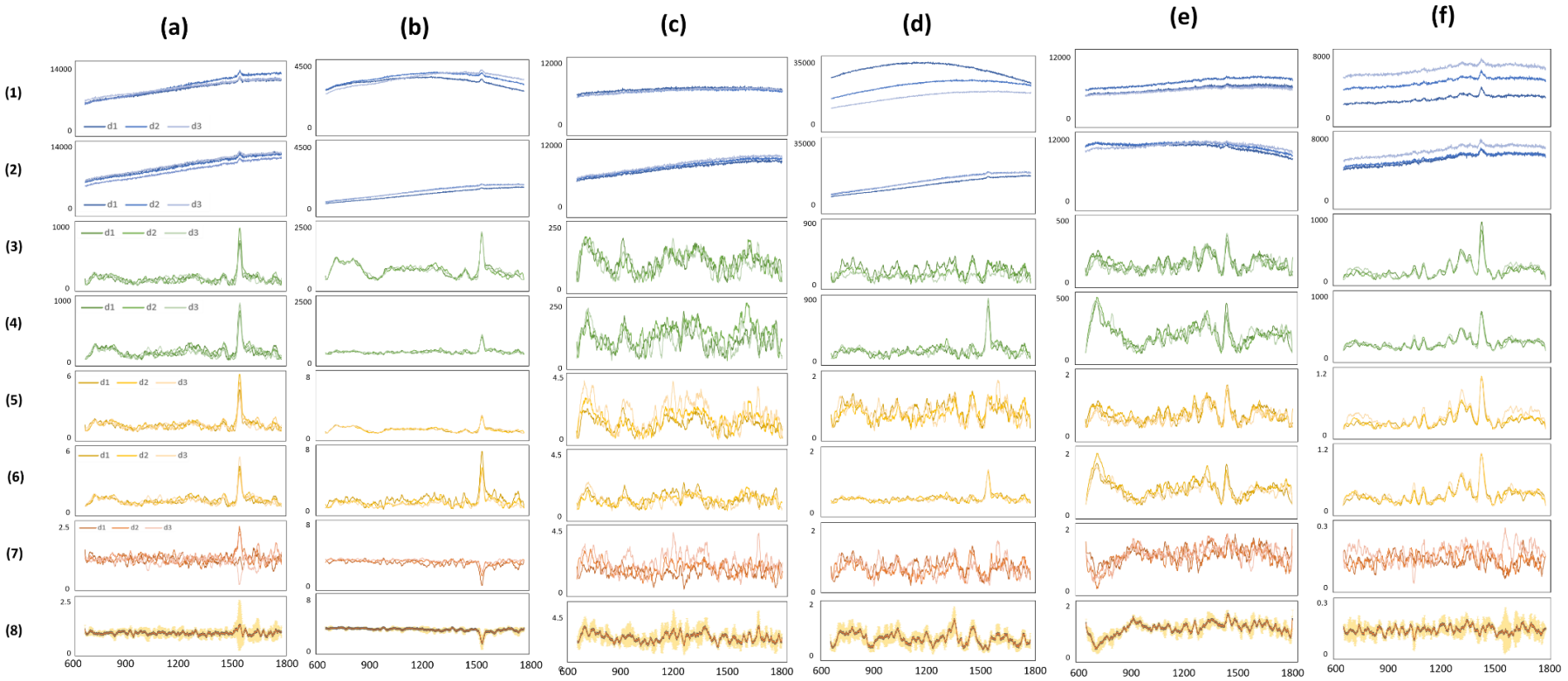

doi:10.6342/NTU202403291

Figure 3-25 The impact of the detection platform fabrication process on the spectrum acquisition of CTB on an enhanced chip with a DOPC-supported lipid bilayer. (a) and (b) upside down measurements on chips treated with Ar-plasma for 10 minutes, using polystyrene microparticles from Bang Laboratories and GmbH, respectively. (c) and (d) upside down measurements on chips treated with Ar-plasma for 10 minutes followed by additional air-plasma treatment for 20 seconds, using polystyrene microparticles from GmbH and Bang Laboratories, respectively. (e) and (f) upside up measurements on chips treated with Ar-plasma for 10 minutes followed by additional air-plasma treatment for 20 seconds, using polystyrene microparticles from Bang Laboratories and GmbH, respectively. process to obtain spectrum of CTB with DOPC containing 1 mol% GM1 on chips. (1)(2) the spectra of (CTB + DOPC(with GM1) + PBS buffer + chip) and (DOPC(with GM1) + PBS buffer + chip) before background removal. (3)(4) the spectra of(CTB + DOPC(with GM1) + PBS buffer + chip) and (DOPC(with GM1) + PBS buffer + chip) after background removal using a 5th-degree polynomial. (5)(6) the spectra of (CTB + DOPC(with GM1) + PBS buffer + chip) and (DOPC(with GM1) + PBS buffer + chip) after background removal using a 5th-degree polynomial, followed by normalization at wavenumber 720 cm^{-1}. (7) the spectrum of CTB obtained by subtracting the spectrum in (6) from the one in (5). (8) average of all spectra in (7).

doi:10.6342/NTU202403291

3.6.2 Comparison of Different Chip Treatments

From **Figure 3-26**, it can be observed that the spectral characteristic peaks of (c) and (d) better match the spectrum of CTB on the chip. The only difference between these two sets of parameters is the brand of polystyrene used; everything else is the same. Firstly, the chips were placed upside down during detection, preventing signal interference from the solution. Secondly, both groups underwent Ar-plasma treatment for 10 minutes followed by Air-plasma treatment for 20 seconds. We speculate that this not only improved the deposition quality of DOPC but also cleaned the chip surface more effectively.

doi:10.6342/NTU202403291

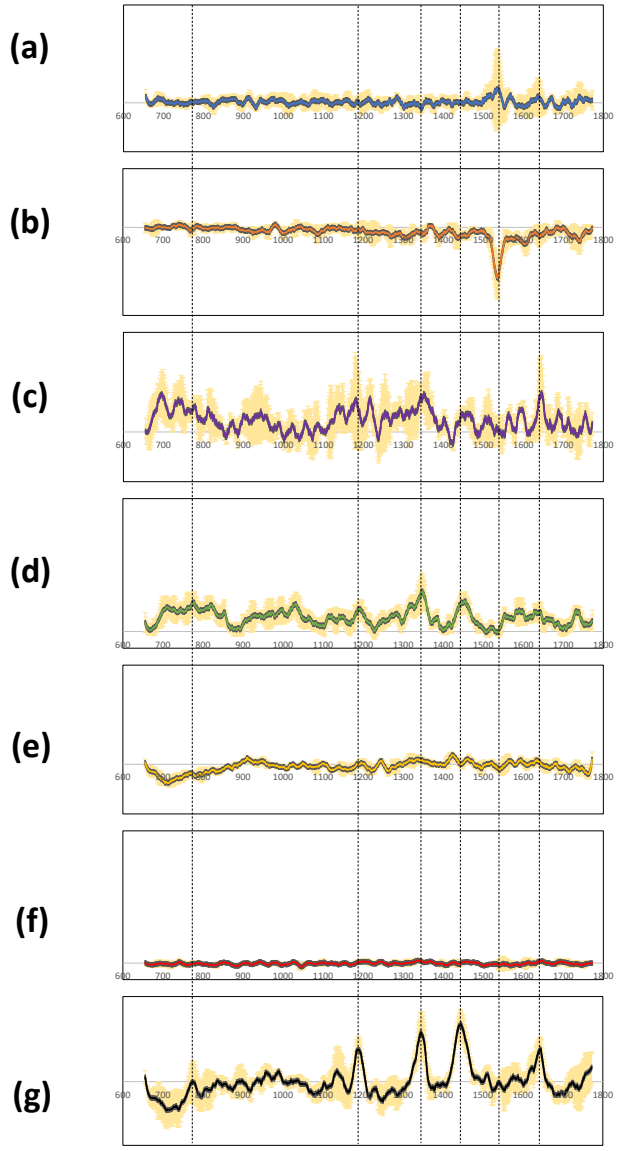

Figure 3-26 Raman spectra of CTB on chips with DOPC containing 1 mol% GM1 obtained with different process parameters, (a) upside down with GmbH chip treated with 10 minutes Ar-plasma before adding DOPC and CTB; (b) upside down with Bang laboratory chip treated with 10 minutes Ar-plasma before adding DOPC and CTB; (c) upside down with GmbH chip treated with 10 minute Ar-plasma + 20 second air-plasma before adding DOPC and CTB; (d) upside down with Bang laboratory chip treated with

doi:10.6342/NTU202403291

10 minute Ar-plasma + 20 second air-plasma before adding DOPC and CTB; (e) up-side up with GmbH chip treated with 10 minute Ar-plasma + 20 second air-plasma before adding DOPC and CTB; (f) upside up with Bang laboratory chip treated with 10 minute Ar-plasma + 20 second air-plasma before adding DOPC and CTB; (g) standard CTB spectrum.

3.7 Performing CTB Detection on a Fabricated Chip with a GPMV Membrane Patch

3.7.1 Impact of the Detection Method and Fabrication Process on the Spectrum Acquisition of CTB on the Chip with a GPMV Membrane Patch

Here, we used a GPMV membrane patch as the detection platform, utilizing the native GM1 on the platform to bind CTB. We employed six different sample preparation methods to understand the impact of air-plasma treatment and chip placement on the detection results.

doi:10.6342/NTU202403291

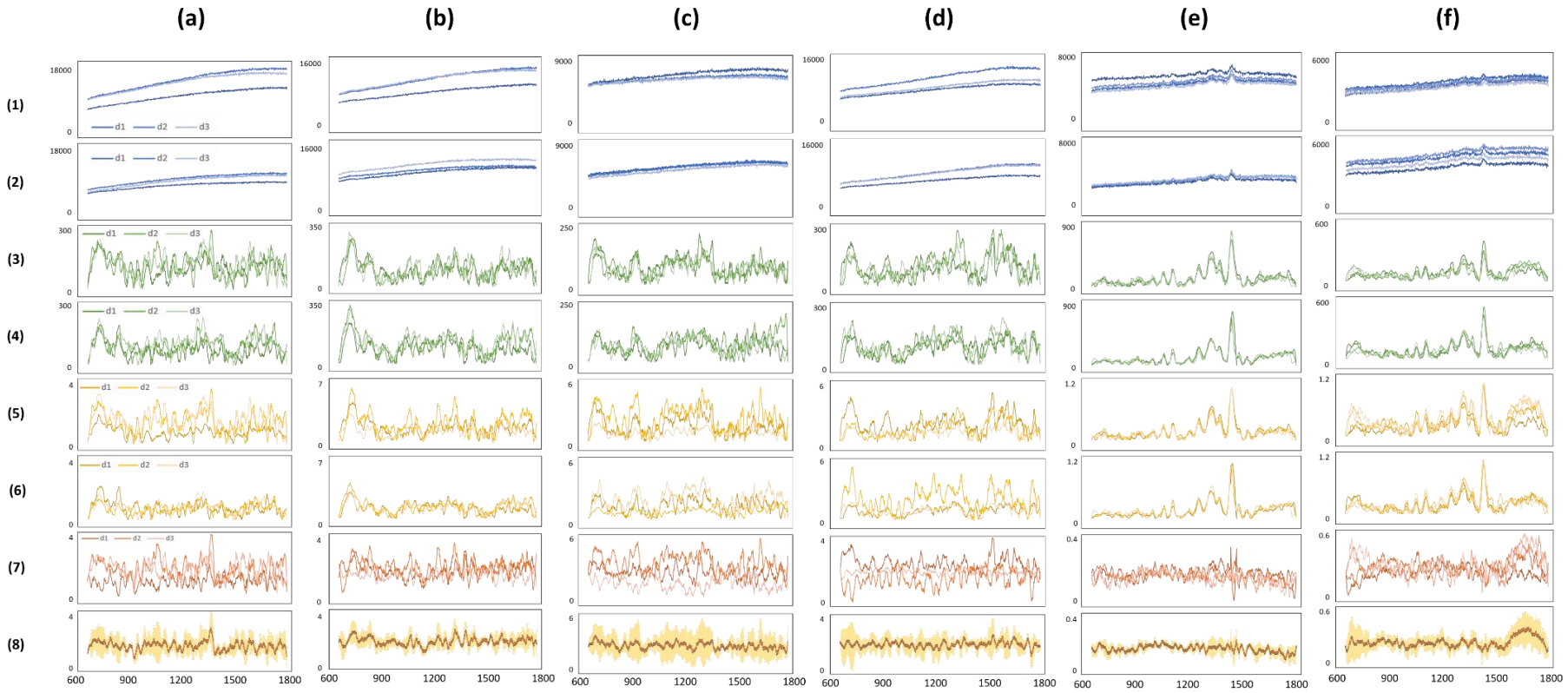

doi:10.6342/NTU202403291

Figure 3-27 The impact of the detection platform fabrication process on the spectrum acquisition of CTB on an enhanced chip with a GPMV membrane patch. (a) and (b) upside down measurements on chips treated with Ar-plasma for 10 minutes, using polystyrene microparticles from Bang Laboratories and GmbH, respectively. (c) and (d) upside down measurements on chips treated with Ar-plasma for 10 minutes followed by additional air-plasma treatment for 20 seconds, using polystyrene microparticles from Bang Laboratories and GmbH, respectively. (e) and (f) upside up measurements on chips treated with Ar-plasma for 10 minutes followed by additional air-plasma treatment for 20 seconds, using polystyrene microparticles from Bang Laboratories and GmbH, respectively. process to obtain spectrum of CTB with GPMV on chips. (1)(2) the spectra of (CTB + GPMV + PBS buffer + chip) and (GPMV + PBS buffer + chip) before background removal. (3)(4) the spectra of (CTB + GPMV + PBS buffer + chip) and (GPMV + PBS buffer + chip) after background removal using a 5th-degree polynomial. (5)(6) the spectra of (CTB + GPMV + PBS buffer + chip) and (GPMV + PBS buffer + chip) after background removal using a 5th-degree polynomial, followed by normalization at wavenumber 1000 cm^{-1}. (7) the spectrum of CTB obtained by subtracting the spectrum in (6) from the one in (5). (8) average of all spectra in (7).

doi:10.6342/NTU202403291

3.7.2 Comparison of Different Chip Treatments

From **Figure 3-28**, it can be observed that none of the parameter tests yielded significant CTB characteristic peaks when detecting CTB on the GPMV membrane patch. We believe this may be because the GPMV membrane patch and the associated CTB are difficult to reach for the electric field enhancement area, thus making CTB detection challenging.

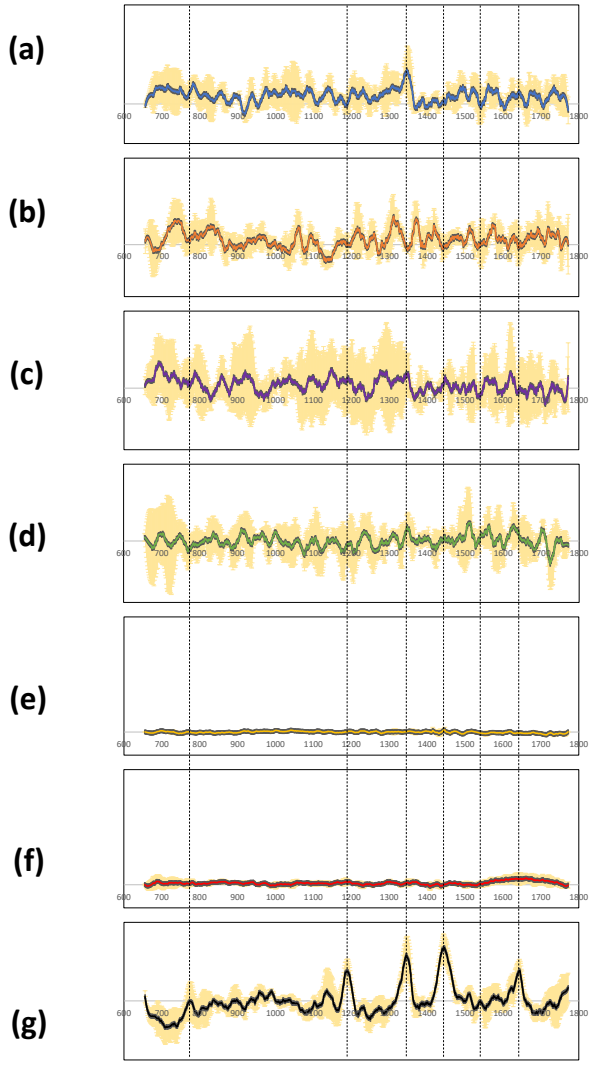

Figure 3-28 Raman spectra of CTB on chips with GPMV obtained with different process

doi:10.6342/NTU202403291

parameters, (a) upside down with GmbH chip treated with 10 minutes Ar-plasma before adding GPMV and CTB; (b) upside down with Bang laboratory chip treated with 10 minutes Ar-plasma before adding GPMV and CTB; (c) upside down with GmbH chip treated with 10 minute Ar-plasma + 20 second air-plasma before adding GPMV and CTB; (d) upside down with Bang laboratory chip treated with 10 minute Ar-plasma + 20 second air-plasma before adding GPMV and CTB; (e) upside up with GmbH chip treated with 10 minute Ar-plasma + 20 second air-plasma before adding GPMV and CTB; (f) up-side up with Bang laboratory chip treated with 10 minute Ar-plasma + 20 second air-plasma before adding GPMV and CTB; (g) standard CTB spectrum.

3.8 Differences in CTB Detection Capabilities with Different Platforms

The detection capability of a chip for CTB depended not only on the structural integrity of the chip itself but also on the amount of CTB that could enter the signal enhancement region. In the "CTB on an Enhanced Chip alone" group, it could be observed from section 3.5.4 that the characteristic peaks of CTB were quite significant under various kinds of conditions. Since the molecular diameter of CTB was 3.5 nm and the

doi:10.6342/NTU202403291

distance between adjacent gold nanotriangle vertices was 30 nm, CTB could easily enter the gaps between the gold nanotriangles. This was the reason why CTB signal detection was effective when only CTB was on the chip. In the "CTB on an Enhanced Chip with a DOPC-supported Lipid Bilayer" group, section 3.6.4 showed that only the designs with conditions (c) and (d) could effectively detect CTB. This confirmed that the chip's additional 20-second Air-plasma treatment allowed better deposition of DOPC supported lipid bilayers in the gaps between the gold nanotriangles, and inverting the chip on the platform avoided solution interference with Raman scattering. In the "CTB on an Enhanced Chip with a GPMV Membrane Patch" group, section 3.7.4 revealed that none of the conditions could effectively detect CTB on the GPMV membrane patch.

Our ultimate goal is to effectively detect CTB on the GPMV membrane patch, but all the groups tested so far have failed to achieve this goal. The diameter of the GPMV patch is approximately 10-20 μm, which is much larger in scale than the gold nanotriangle. Additionally, cholesterol helps maintain a certain tension in the cell membrane, preventing it from collapsing. Therefore, when the vesicle breaks on the chip surface, it tends to span over the gold nanotriangles. According to the schematic of CTB in the system (**Figure 3-29**), we believe that this chip only generates localized electric field enhancement on the sides of the gold nanotriangles. The localized electric field

doi:10.6342/NTU202403291

enhancement effect above the gold nanotriangles may be very weak, which is likely why CTB could not be detected by the Raman instrument.

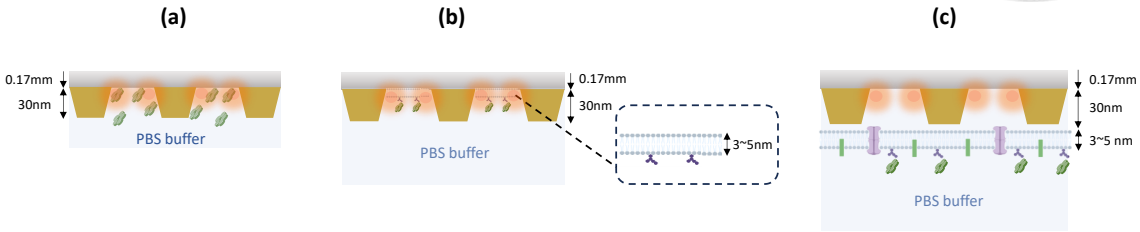

Figure 3-29 Schematic diagram of CTB in different systems and its relative position to the electric field enhancement region (a) CTB on a fabricated chip alone (b) CTB on a fabricated chip with a DOPC-supported lipid bilayer (c) CTB on a fabricated chip with a GPMV membrane patch.

Chapter 4 Conclusion

We successfully established a detection platform based on Raman technology with supported cell membranes to study events on cell membranes. By using gold nanotriangle structure chips formed by colloidal lithography, we enhanced the signals of cell membranes and their interacting substances, enabling the detection of cholera toxin subunit B (CTB) and the 1,2-dioleoyl-sn-glycero-3-phosphocholine (DOPC) lipid bilayer. However, the giant plasma membrane vesicle (GPMV) patches exhibited weak signals inconsistent with the standards, likely due to the inability of the GPMV patches to fall

doi:10.6342/NTU202403291

into the narrow enhancement areas of the chip. Further experiments using DOPC lipid bilayers with monosialotetrahexosylganglioside (GM1) and GPMV patches with natural receptors demonstrated that while CTB captured on the DOPC lipid bilayer could be detected, the CTB signal from the GPMV patch remained weak. This result aligns with our hypothesis that CTB adheres to the DOPC lipid bilayer within the enhancement areas, but remains far from the signal enhancement area when attached to the GPMV patch, rendering it undetectable with the current chip configuration.

References

1. Bretscher, Mark S., et al., *The molecules of the cell membrane*. Scientific American,1985. 253(4): p. 100.
2. Kenworthy, A.K., et al., *Cholera toxin as a probe for membrane biology.* Toxins, 2021. 13(8): p. 543.
3. Lai, C., et al., *Determination of the primary structure of cholera toxin B subunit.* Journal of Biological Chemistry, 1977. 252(20): p. 7249.
4. Guicheteau, J., et al., *Raman and surface-enhanced Raman spectroscopy of amino acids and nucleotide bases for target bacterial vibrational mode identification*. *Chemical and Biological Sensing VII*, 2006. Vol. 6218: p. 174.

doi:10.6342/NTU202403291

5. Zhu, Guangyong, et al., Raman spectra of amino acids and their aqueous solutions. *Spectrochimica Acta Part A: Molecular and Biomolecular Spectroscopy*, 2011. 78(3): p. 1187.

6. Jenkins, Amanda L., Richard A. Larsen, and Timothy B. Williams, et al., Characterization of amino acids using Raman spectroscopy. *Spectrochimica Acta Part A: Molecular and Biomolecular Spectroscopy*, 2005. 61(7): p.1585.

7. Triggs, Nancy E., and James J. Valentini, et al., An investigation of hydrogen bonding in amides using Raman spectroscopy. *The journal of physical chemistry*, 1992. 96(17): p.6922.

8. Sane, Samir U., Steven M. Cramer, and Todd M. Przybycien, et al., A holistic approach to protein secondary structure characterization using amide I band Raman spectroscopy. *Analytical biochemistry*, 1999. 269(2): p.255.

9. Matthews, J.R., et al., *Structural Analysis by Enhanced Raman Scattering.* Nano Lett, 2017. 17(4): p. 2172.

10. Kühler, P., M. Weber, and T. Lohmüller., et al., *Plasmonic nanoantenna arrays for surface-enhanced Raman spectroscopy of lipid molecules embedded in a bilayer membrane.* ACS applied materials & interfaces, 2014. 6(12): p. 8947.

11. Mrđenović, D., et al., *Nanoscale Chemical Imaging of Human Cell Membranes Using Tip-Enhanced Raman Spectroscopy.* Angewandte Chemie, 2022. 134(43):

doi:10.6342/NTU202403291

e202210288 p. 1.

12. Hodges, M.D., et al., *Combining immunolabeling and surface-enhanced Raman spectroscopy on cell membranes.* ACS nano, 2011. 5(12): p. 9535.

13. Syed, A. and E.A. Smith., et al., *Raman imaging in cell membranes, lipid-rich organelles, and lipid bilayers.* Annual Review of Analytical Chemistry, 2017. 10(1): p. 271.

14. Böhme, R., et al., *Biochemical imaging below the diffraction limit–probing cellular membrane related structures by tip-enhanced Raman spectroscopy (TERS).* Journal of Biophotonics, 2010. 3(7): p. 455.

15. Raffy, S. and J. Teissié., et al., *Control of lipid membrane stability by cholesterol content.* Biophysical journal, 1999. 76(4): p. 2072.

doi:10.6342/NTU202403291

doi:10.6342/NTU202403291